electronics

MDPI

Article

Protection Channel Competition and Network Feedback in Correlated Converter Disconnections

Fan Li [1], Jishuo Qin [1,2,*], Hanqing Liang [1], Jian Meng [1], Rui Shi [3] and Guodong Guo [1]

[1] State Grid Economic and Technology Research Institute Co., Ltd., Beijing 102209, China; lifan658@163.com (F.L.); lianghanqing@chinasperi.sgcc.com.cn (H.L.); mengjian@chinasperi.sgcc.com.cn (J.M.); guoguodong@chinasperi.sgcc.com.cn (G.G.)
[2] School of Electrical and Electronic Engineering, North China Electric Power University, Beijing 102209, China
[3] State Grid Corporation of China, Beijing 100031, China; shirui@sgcc.com.cn
* Correspondence: js-qin@ncepu.edu.cn

Abstract

After a fault on a weak network is cleared, several grid-following converters sharing a common bus can disconnect in quick succession. Which units disconnect, and through which protection, depends on competing AC and DC overvoltage functions, on the memory of measurement filters and timers, and on the voltage change caused by the first disconnection; a voltage-peak check or a prescribed outage list cannot capture these interactions. This paper proposes a model-specific diagnostic framework that carries converter states, filtered measurements, timer ages, and connection states from one protection event to the next and explains the outcomes by three conditions: the voltage change caused by a disconnection, the completion or reset of a pending timer, and the DC energy remaining after blocking. All combinations of bounded AC setting changes are re-simulated in closed loop on a three-converter positive sequence benchmark. Raising AC thresholds never increased the number of disconnected units, which is a structural property of this benchmark rather than a physical guarantee. However, in 830 of 23,328 single-setting comparisons, it shifted the disconnection to another unit and in 40 from the AC to the DC protection of the same unit; separate setting changes did not have additive effects. A fixed-topology relay evaluation identified different disconnected units in 613 of 5832 runs, which demonstrates a logical necessity check within the same equations rather than evidence that the full model is physically more accurate. Under the averaged model, the relief given by the first disconnection depends strongly on the assumed current interruption law. The findings lack EMT or hardware validation and yield neither protection settings nor outage probabilities.

Keywords: converter protection; correlated disconnection; fault ride-through; protection timer; DC-link overvoltage; network feedback; grid-following converter

Check for updates

Academic Editor: Fabio Corti

Received: 9 October 2026
Revised: 26 October 2026
Accepted: 26 October 2026
Published: 29 October 2026

Copyright: © 2026 by the authors. Licensee MDPI, Basel, Switzerland. This article is an open access article distributed under the terms and conditions of the Creative Commons Attribution (CC BY) license.

1. Introduction

1.1. Engineering Motivation

The increasing use of power electronic interfaces changes both the continuous response to a grid disturbance and the conditions under which generating units cease injecting current. Converter control and grid synchronization provide the basic connection between terminal measurements and current injection [1]. Their stability depends on the network and on the synchronization and control dynamics retained in the model [2]. Disturbance assessment must also respect voltage, current, and energy constraints because satisfactory synchronization alone does not establish safe converter operation [3]. For a group of

converters exposed to one fault, the practical question is consequently broader than whether one control loop remains stable: which units disconnect, which protection channels initiate those disconnections, and whether an earlier disconnection changes the subsequent actions of the other units.

The situation examined here is a group of grid-following converters connected through individual feeders to the common bus of a weak network. A source-side fault depresses the bus voltage, and each converter raises its reactive current to support it. During the fault, the converters cannot export their full active power, so energy accumulates in their DC-link capacitors. At fault clearing, the source voltage returns while the reactive current is still high because the control measurement and the current loop respond with their own time constants; the result is a temporary overvoltage at the converter terminals. Two protective functions then compete in each unit: an AC overvoltage function that acts on a filtered terminal voltage after a definite time, and a DC overvoltage function that acts on the accumulated capacitor energy. When the first unit blocks its converter, its current disappears from the common bus, and the terminal voltages of the other units change instantaneously by an amount fixed by the grid impedance and the withdrawn current. Whether the other units then disconnect depends on their filtered measurements, on the exceedance time their timers have already accumulated, and on the subsequent closed-loop response. These interactions, rather than any single voltage peak, determine the set of disconnected units and the initiating function of each.

Three distinctions are essential. Preventing the operation of an AC protective function does not establish that a DC protective function will remain inactive. A decline in terminal voltage following the first disconnection does not erase the measurement and timing states already accumulated in another unit. Finally, withdrawal of AC current does not instantaneously remove the energy supplied to the disconnected converter's DC capacitor. An assessment that combines these three questions into a single connected or disconnected outcome can report an apparent improvement while missing a different channel, a different device, or a post-blocking voltage violation.

1.2. Related Work and the Remaining Gap

Fault ride-through studies provide a direct basis for retaining several restrictions in the same assessment. Mirhosseini et al. considered disconnection problems associated with DC-link voltage, AC current, and grid voltage synchronization in photovoltaic converters [4]. Ding et al. developed DC-link voltage control for two-stage photovoltaic inverters during low-voltage ride-through [5]. Wang and Ren investigated coordinated DC-side and grid-side control to improve fault ride-through [6]. These studies explain why AC terminal behavior cannot be interpreted independently of DC-side energy accumulation. They do not imply that suppressing one protection action eliminates every other reason for the same converter to disconnect; that implication requires calculation of the changed closed-loop trajectory.

Synchronization research demonstrates the importance of retaining the relevant continuous dynamics. Taul et al. compared assessment methods under severe symmetrical faults and distinguished the existence of an equilibrium from transient synchronization stability [7]. Wu and Wang developed a design-oriented analysis of PLL-synchronized converters [8]. Zhao et al. examined nonlinear PLL operation and the associated transient operating region [9]. He et al. related low-voltage ride-through instability to the interaction between terminal voltage and PLL dynamics [10]. Hu et al. included current control interaction in an equivalent synchronization model [11]. Under asymmetrical faults, positive- and negative sequence interactions introduce additional restrictions [12]. A recent review likewise emphasizes the dependence of grid-following transient stability on control structure and grid-converter interactions [13]. These results motivate an explicit model

boundary: the benchmark used here retains current, phase, measurement, and DC energy dynamics, but does not represent a manufacturer's complete synchronization controller, negative sequence control, or switching process.

Protection and limiting behavior also depend on converter implementation. Banaiemoqadam et al. designed dual current control to support correct protective relay operation [14]. Fan et al. reviewed the relationship among current limitation, fault current contribution, and recovery in grid-forming inverters [15]. Zhang et al. used set–reset latches in a dynamic current limitation strategy [16]. Bottrell and Green experimentally compared instantaneous and latched current limitation with different reset choices, demonstrating the significance of internal controller state [17]. Ordono et al. identified current limitation as a central part of low-voltage ride-through behavior [18]. Reactive current support in weak networks remains an active topic, as illustrated by Gwon and Choi's study under a low weighted short-circuit ratio [19]. Although these papers concern different control and protection functions, they support preserving the memory of each implemented element. In this study, that memory comprises filtered measurements, uninterrupted exceedance timers, and trip latches that remain set throughout the observation interval.

At the system level, protection actions have long been recognized as contributors to multiple outages. Phadke examined hidden failures that remain unobserved in normal operation and become consequential during disturbances [20]. Chen et al. studied cascading behavior using a transmission network model that includes protection-related hidden failures [21]. Song et al. showed the value of jointly simulating network and protection dynamics when investigating cascading mechanisms [22]. Hines et al. established that outage influence relationships need not coincide with physical network topology [23]. Statistical studies of blackout sequences address the complementary problem of characterizing distributions over event ensembles [24]. Nakarmi et al. surveyed interaction graph methods for outage dependence [25]. Here, competition between explicitly represented protection functions is not assumed to be a protection defect. A short interval between two disconnections is treated as an observed ordering; it does not by itself establish that the first caused the second.

Operating condition uncertainty introduces a further distinction. Renewable generation scenario methods can represent variability in the operating points supplied to a security study [26]. A deterministic parameter scan instead identifies outcomes at the evaluated points. Without justified disturbance frequencies and scenario weights, the fraction of points with an outcome is not an occurrence probability. The present calculations therefore report conditional action sets, disconnected capacity, and power deficit integrals.

Taken together, the studies above supply the individual ingredients of the present assessment: filtered measurements, definite-time timers, AC/DC channel competition, and post-blocking energy checks. What they do not supply, on a common test case, is a comparison in which each protection setting change is followed by a new closed-loop solution, pending timers retain their physical history, and the DC energy remains subject to its limit after the AC injection has ceased. A common simplification in multi-outage studies evaluates each protection criterion on the trajectory of the unchanged topology and then prescribes the resulting outage list; the electrical feedback of the first action on the remaining units is then absent. The present work is therefore a model-specific diagnostic framework rather than a new protection theory: the network, filter, and energy identities it uses are elementary, and their role is to provide explicit, testable conditions for interpreting the coupled protection outcomes. In the terminology of hybrid dynamical systems [27], the converter trajectories evolve continuously between protection events, while the connection states, timer ages, and latches change at guard crossings; the formulation of Section 2 adopts this description. A fixed-topology relay evaluation of the kind described above is included

in Section 6 as a comparison on the same test case. Because that evaluation uses the same equations, the comparison shows what the omission of network feedback implies within the model; it does not by itself show which model is closer to physical reality.

1.3. Research Questions, Contributions, and Paper Organization

The research questions are as follows: for a given fault and operating point, which converters disconnect, through which protective function, and how does the first disconnection change the subsequent actions of the others? The paper answers these questions within a constructed benchmark through three connected elements.

The first element is a hybrid state formulation of correlated disconnections with explicit AC/DC channel competition. It specifies the state that must be carried from one protection event to the next: continuous converter states, filtered measurements, timer ages, connection states, and first-cause latches. Within this formulation, three conditions address the three distinctions stated above. A network voltage jump relation, exact within the retained algebraic network, gives the sign and size of the instantaneous electrical effect of one disconnection on the other terminals. Conditional timer bounds translate that effect into whether a pending AC timer of a surviving unit completes or resets; they are interpretive tools applied after direct integration, not a predictive substitute for it. A residual energy relation checks the DC voltage of the blocked unit after its AC injection has ceased, including a critical source exit time constant. The three conditions thus correspond, in order, to the peer unit's pending AC action, the modified unit's competing DC action, and the blocked unit's post-action equipment limit.

The second element quantifies how often these mechanisms change the outcome. Complete combinations of bounded local AC setting changes are evaluated by re-solving the closed-loop trajectory for each combination. Device identities and first causes are retained even when the total disconnected unit count is unchanged, and second- and third-order setting differences quantify when the effects of separate local changes fail to add.

The third element bounds the conclusions. The evaluation includes protection model comparisons, among them a fixed-topology relay evaluation without network feedback, which serves as a logical necessity check within the same equations rather than as external validation; continuous event verification; full-grid variations of the synchronization model, the control voltage floor, and the current interruption time; and two pre-specified sensitivity sets whose settings and operating points were fixed by rule before evaluation but which belong to the same benchmark. Results that contradict a universal interpretation are retained, including the loss of a suppressive feedback effect when current withdrawal is delayed. The findings are finally classified as invariant within the retained model, which is a statement about the retained equations and the evaluated grids rather than about physical robustness; model-dependent; or requiring detailed electromagnetic transient (EMT) or hardware validation. The study establishes conditional mechanisms and measured model sensitivity rather than protection setting optimality, physical robustness, or complete reachability over unknown continuous parameters.

Section 2 defines the converter network and protection states and their physical meaning. Section 3 derives the network, timer, and residual energy conditions. Section 4 describes the intervention comparisons and assessment quantities. Section 5 specifies the experiments, the implementation, and the numerical checks. Section 6 presents the results. Section 7 discusses the engineering interpretation, classifies the findings by the evidence that supports them, and states the limitations. Section 8 concludes the paper.

2. Converter Network Model and Protection States

This section establishes the retained electrical and protection dynamics. The network equations connect the converters through a common bus; current and source power controls determine their continuous trajectories; and measurement filters, timers, and latches determine disconnection. The model is a constructed positive sequence benchmark designed to expose interactions among these quantities. It is not an electromagnetic transient representation of semiconductor switching or a calibrated plant model.

Each converter represents an aggregated grid-following plant: a current-controlled voltage source converter whose active and reactive current components i_{di} and i_{qi} follow their references in a synchronous frame aligned by a synchronization loop with angle θ_i; a DC link whose capacitor holds the normalized energy w_i and is fed by a source-side input power p_{si}, for example, from a photovoltaic or machine-side stage; and a feeder impedance to the common bus. Three measurements are retained because they serve different functions: a control measurement $\hat{v}_i$ that sets the reactive current support, an AC protection measurement y_{Ai} that represents the measuring window of a numerical overvoltage relay, and a DC protection measurement y_{Di} of the DC-link voltage. The protective functions are an AC overvoltage function and a DC overvoltage function, each with a definite time delay, together with hard limits on AC voltage, DC voltage, and current that represent the withstand capability of the equipment. Disconnection is converter blocking, which is the removal of the switching pulses: the current references and the source input target are set to zero, the connection state is latched, and no restart is allowed within the observation window.

The assessment state is hybrid in the following sense. It consists of the continuous states listed above together with the discrete connection state b_i, the timer ages a_{Ai} and a_{Di}, and the first-cause identifier r_i of each unit. The continuous states evolve between protection events, and the discrete states change at guard crossings; this is the description of a hybrid dynamical system [27], and the term hybrid state is used in this sense throughout. Table 1 lists the principal symbols.

Table 1. Principal symbols and quantities used in the assessment.

Symbol	Physical Meaning	Unit
s_i, b_i	Capacity weight; connection state	dimensionless
I_i, V_i, V_b	Converter current; terminal and common bus voltage	p.u.
i_{di}, i_{qi}, θ_i	Current components and synchronization angle	p.u.; rad
w_i, p_{si}, p_{aci}	Squared DC voltage; input and output power	p.u.
y_{Ai}, y_{Di}, $\hat{v}_i$	AC/DC protection and control measurements	p.u.
a_{ri}, d_r, ρ_{ri}	Timer age, required delay, and remaining time	s
T_E, T_b, T_A	Energy, source exit, and AC measurement constants	s
η_{ri}, V_H, V_{DH}, I_H	Soft thresholds and hard limits	p.u.
N, C, D	Disconnected unit count, capacity fraction, power deficit integral	count; p.u.; p.u. s

2.1. Network and Per-Unit Convention

Each converter uses its own rated power as the active power and current base, with a common voltage base. The capacity weight $s_i = S_i/S_B$ converts its injection to the system base, where S_i is the converter rating and $S_B = \sum_i S_i$. The binary connection state b_i equals one before blocking and zero afterward. The complex injected current is defined by

$$I_i = b_i(i_{di} - ji_{qi})e^{j\theta_i}. \tag{1}$$

where i_{di} and i_{qi} are the active and reactive current components in the converter reference frame, θ_i is its phase angle in radians, and $j^2 = -1$. Positive i_{qi} gives the reactive current

convention used by the benchmark. The normal and faulted source voltages enter the algebraic network through

$$V_b = E_g + Z_g \sum_{i=1}^{n} s_i I_i, V_i = V_b + Z_i I_i, p_{aci} = \Re\{V_i I_i^*\}. \quad (2)$$

where E_g is the external source voltage, $Z_g = R_g + jX_g$ is the common grid impedance on the system base, and $Z_i = R_i + jX_i$ is the feeder impedance on converter i's base. V_b and V_i denote the common bus and converter terminal voltages, and p_{aci} is the converter active power injection on its own base. The sign of the voltage drop expression follows the current direction from the converters toward the source.

The network balance used to check the numerical implementation follows directly from Equation (2):

$$\sum_i s_i p_{aci} = \Re\{E_g I_g^*\} + R_g |I_g|^2 + \sum_i s_i R_i |I_i|^2, I_g = \sum_i s_i I_i. \quad (3)$$

where I_g is the common grid current on the system base. This equality checks the consistency of the retained network and its per-unit conversions. A small residual does not validate omitted network dynamics.

2.2. Current Control, Synchronization, and DC Energy

The converter raises its reactive current reference during a voltage depression. A floor on the control measurement prevents division by a voltage close to zero; its value of 0.05 p.u. is a modeling choice. Over the evaluated parameter grid, the control measurement never falls below 0.419 p.u., so the floor is inactive; its one-factor sensitivity, including a value at which it binds, is reported in Section 6.9. The reactive current priority reference is

$$\overline{v}_i = max\{\hat{v}_i, 0.05\}, i_{qi}^* = clip\Big\{K_q(v_{i0} - \overline{v}_i), 0, I_{max}\Big\}. \quad (4)$$

where $\hat{v}_i$ is the control voltage measurement, v_{i0} is the initialized terminal magnitude, K_q is the reactive current gain, and $clip\{a,l,u\} = min\{u,max\{l,a\}\}$. All voltages and currents in Equation (4) are in per unit. The remaining current capacity is assigned to active power according to

$$p_i^* = max\{0, p_{i0} + k_E(w_i - 1)\}, i_{di}^* = min\left\{\frac{p_i^*}{\overline{v}_i}, \sqrt{I_{max}^2 - \left(i_{qi}^*\right)^2}\right\}. \quad (5)$$

where p_{i0} is the initial active power, $w_i = v_{dci}^2$ is normalized DC energy, and k_E is the gain that increases active power extraction when DC energy rises. The closed-loop current and phase dynamics are

$$T_I \dot{i}_{di} = i_{di}^* - i_{di}, T_I \dot{i}_{qi} = i_{qi}^* - i_{qi}, \dot{\theta}_i = k_{\mathrm{PLL}} \Im\left\{V_i e^{-j\theta_i}\right\}. \quad (6)$$

where T_I is the current response time constant in seconds and k_{PLL} is the phase-response gain. The phase model is a first-order synchronization equivalent in which the angle rate is proportional to the quadrature voltage $\Im\left\{V_i e^{-j\theta_i}\right\}$. A synchronous reference frame phase-locked loop (PLL) with a proportional–integral regulator adds an integrator state and gives a second-order closed loop [28]; this variant is defined in Section 5.2 and evaluated on the full parameter grid in Section 6.9, so that the dependence of the protection outcomes on the synchronization model is measured rather than assumed. The current reference remains in the disk of radius I_{max}. Because a first-order response is a positive weighted combination of its initial state and reference history, a current state initialized in this disk remains in it. This is a property of the averaged current model, not a semiconductor overcurrent guarantee.

Separate measurements are retained for control and protection:

$$T_v\dot{\hat{v}}_i = |V_i| - \hat{v}_i, T_A\dot{y}_{Ai} = |V_i| - y_{Ai}, T_D\dot{y}_{Di} = \sqrt{w_i} - y_{Di}. \quad (7)$$

where y_{Ai} and y_{Di} are the AC and DC protection measurements, and T_v, T_A, and T_D are their time constants. Treating these three measurements as identical would change both reactive current support and the sequence of protection actions.

The DC capacitor retains the mismatch between source input and AC output:

$$T_E\dot{w}_i = p_{si} - p_{aci}, T_s\dot{p}_{si} = p_{si}^{\text{tar}} - p_{si}. \quad (8)$$

where $T_E = E_{dc,0}/S_i$ is the DC energy time constant in seconds, $E_{dc,0}$ is the initial capacitor energy, and p_{si} is the source-side input power on the converter base. Before blocking, the source reduces input continuously as DC voltage rises:

$$p_{si}^{\text{tar}} = p_{i0}clip\left\{1 - \frac{\sqrt{w_i} - v_f}{\Delta v_f}, 0, 1\right\}. \quad (9)$$

where v_f is the foldback starting voltage and Δv_f is its voltage span. Blocking sets both current references and the source target to zero and changes the source time constant to T_b. The current controller states subsequently decay, while Equation (1) removes the port injection immediately in the baseline model. The DC state continues to evolve throughout the observation interval.

Figure 1 summarizes the retained components and computation sequence. The separation between AC current withdrawal and source power withdrawal is explicit; it permits a post-blocking energy check without assuming that disconnection instantaneously makes the DC state stationary.

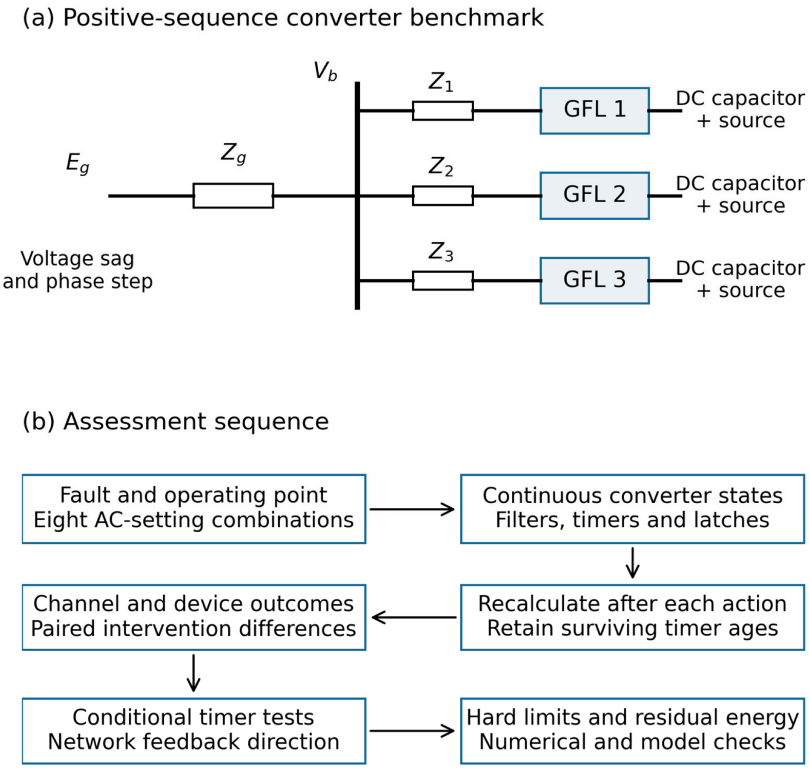


Figure 1. Converter network benchmark and assessment sequence: (**a**) common grid and feeder connections with converter-side energy storage; (**b**) calculation of trajectories, intervention differences, and protection state conditions.

2.3. Timers, Competing Channels, and Latches

The soft AC and DC functions operate on filtered measurements. Their guard excesses are

$$g_{Ai} = y_{Ai} - \eta_{Ai}, g_{Di} = y_{Di} - \eta_{Di}. \tag{10}$$

where η_{Ai} and η_{Di} are the corresponding thresholds. While the device remains connected, each timer measures uninterrupted positive guard duration. For channel $r \in \{A,D\}$, its age is

$$a_{ri}(t) = \begin{cases} t - t_{ri}^{\text{on}}, & g_{ri}(s) > 0 \text{ for all } s \in (t_{ri}^{\text{on}}, t], \\ 0, & g_{ri}(t) \le 0, \end{cases} \tag{11}$$

where t_{ri}^{on} is the start of the current uninterrupted exceedance. A return to or below the threshold resets the age to zero. This definition is not an accumulation of separated exceedance intervals. The alternative hold rule is examined only as a stated model variation.

These semantics correspond to the definite time overvoltage characteristic of numerical relays: the timer starts when the measured quantity exceeds the pick-up value, runs for the set delay, and resets when the measured quantity drops out, while the measuring window of the relay determines how quickly the measured quantity follows the terminal voltage [29,30]. The first-order filter with time constant T_A stands in for that window, and a relay with an intentional reset delay corresponds to the hold variant. The practical consequence is that a protective function can operate after the instantaneous terminal voltage has already fallen below its threshold: the measured quantity lags the terminal voltage, and the timer retains the exceedance duration already accumulated. Section 3.2 quantifies this lag.

For a connected unit, the first completed soft timer or hard-bound violation initiates blocking. The action time is represented by

$$\begin{aligned} t_i = inf\{t : b_i(t^-) = 1,\ a_{Ai} \ge d_A \ \vee\ a_{Di} \ge d_D \vee |V_i| > V_H \\ \vee \sqrt{w_i} > V_{DH} \vee |I_i| > I_H\}. \end{aligned} \tag{12}$$

where d_A and d_D are the soft delays, and V_H, V_{DH}, and I_H are the hard AC voltage, DC voltage, and current limits. The first-cause identifier is retained separately from the connection state. At an exact simultaneous numerical completion, the fixed-step implementation gives priority to hard current, hard DC voltage, hard AC voltage, soft DC, and soft AC, in that order. Such ties do not justify an inferred physical causal ordering.

After an action, b_i remains zero; no automatic restart is allowed. The continuous current, phase, measurement, energy, and source power states are not reset. The states of surviving devices, including their timer ages, also continue. The action sequence generated by a fault c and parameter vector ϑ is

$$\Pi(c, \vartheta) = \{(i_k, r_k, t_k)\}_{k=1}^{K}, 0 \le K \le n. \tag{13}$$

where i_k, r_k, and t_k identify the disconnected unit, initiating channel, and action time. Equal-time actions form one simultaneous group. Each successive electrical interval is calculated with the connection state produced by the preceding group; later actions are not imposed from a prescribed outage list.

The timer age is necessary to reconstruct the next action even when terminal voltage and the connection set are known. Similarly, the source power state is necessary to assess DC voltage after current injection has ceased. These quantities distinguish the assessment state from a graph containing only the most recent disconnected device.

3. Network Feedback and Protection State Conditions

This section derives conditions that explain how one protection action changes the opportunity for another. It first determines the instantaneous voltage change caused by

current withdrawal. It then combines this change with measurement and timer memory. Finally, it integrates the energy remaining after blocking. The conditions are exact or sufficient within the retained model; their numerical use preserves an unresolved outcome when the required assumptions or margins are unavailable. They are applied after direct integration as interpretive checks of individual outcomes: every outcome classification reported in Section 6 is obtained from the integrated trajectories themselves, and the conditions explain why those outcomes arise.

3.1. Electrical Sign of a Disconnection

Consider the blocking of unit j at t_k, with no simultaneous source voltage change. Continuous states remain unchanged at that instant. For a surviving unit $i \neq j$, Equation (2) gives the voltage change, which is exact within the algebraic positive sequence network.

$$\Delta V_i = V_i(t_k^+) - V_i(t_k^-) = -Z_g s_j I_j(t_k^-). \tag{14}$$

The feeder drop of the surviving unit is unchanged instantaneously. The squared magnitude change is therefore

$$\left|V_i(t_k^+)\right|^2 - \left|V_i(t_k^-)\right|^2 = -2\Re\left\{V_i\left(t_k^-\right)^* Z_g s_j I_j\left(t_k^-\right)\right\} + \left|Z_g s_j I_j(t_k^-)\right|^2. \tag{15}$$

The sign is determined by the balance of the cross term and the nonnegative quadratic term. Writing $J = Z_g s_j I_j(t_k^-)$, voltage magnitude decreases precisely when $2\Re\{V_i(t_k^-)^* J\} > |J|^2$. The sign is not fixed by the fact that a converter disconnects. For a simultaneous group, $s_j I_j$ is replaced by the sum over the disconnected units. Equations (14) and (15) describe the electrical jump only. The subsequent trajectory includes current control, phase, and energy responses, and a decrease in raw voltage need not prevent a pending protection action.

3.2. Conditional Continuation and Reset of a Pending Timer

Suppose an AC timer is active immediately after a network action. Let its measurement be $y_0 > \eta_A$, its retained age be $a_0 < d_A$, and its remaining duration be $\rho = d_A - a_0$. For a terminal magnitude $v(s)$ on the ensuing fixed-topology interval, Equation (7) has the exact solution

$$y(s) = y_0 e^{-s/T_A} + \frac{1}{T_A}\int_0^s e^{-(s-u)/T_A} v(u)du, \; 0 \le s \le \rho. \tag{16}$$

where $s = t - t_k$. The kernel is positive, so lower and upper bounds on terminal voltage give corresponding measurement bounds. If $\underline{v} \le v(s) \le \overline{v}$ throughout this interval, the measurement satisfies

$$y^-(s) = \underline{v} + (y_0 - \underline{v})e^{-s/T_A} \le y(s) \le \overline{v} + (y_0 - \overline{v})e^{-s/T_A} = y^+(s). \tag{17}$$

The constant input bounds are monotone between their initial and terminal values. Consequently, the following two inequalities provide sufficient decisions for the pending exceedance episode:

$$min\{y_0, y^-(\rho)\} > \eta_A \Rightarrow \text{timer completion}, \; y^+(\rho) < \eta_A \Rightarrow \text{timer reset before expiry}. \tag{18}$$

The completion statement assumes that no competing DC or hard function blocks the device earlier or takes priority at the same instant. The reset statement concerns this uninterrupted episode; it does not exclude a later new exceedance. Neither statement applies across an unaccounted network or source switch. If neither inequality holds, the decision is unresolved and direct integration continues. Equality is treated as unresolved because it has no strict separation from the threshold.

The completion statement has a direct physical reading. Suppose that the terminal voltage drops to a constant value $v < \eta_A$ immediately after the network action, as it does when a disconnection lowers the common bus voltage. The measurement then decays as $y(s) = v + (y_0 - v)e^{-s/T_A}$ and remains above the threshold for

$$s < T_A \ln \frac{y_0 - v}{\eta_A - v}. \tag{19}$$

A pending timer whose remaining duration ρ is shorter than this lag completes even though the terminal voltage is already below the threshold; a timer with a longer remaining duration resets. With $T_A = 2$ ms, a measurement 0.02 p.u. above a threshold that the terminal voltage undershoots by 0.05 p.u. remains above the threshold for 0.67 ms. Equations (18) and (19) are therefore interpretive: from the state at the action instant and the subsequent voltage envelope, they explain why a completed timer under sub-threshold terminal voltage is a consequence of measurement lag and retained timer age rather than a numerical artifact. They do not replace integration of the trajectory, from which every classification in Section 6 is obtained.

Input bounds can be obtained without future waveform extrema when a valid voltage slope bound is available. With $v_0 = |V_i(t_k^+)|$ and $|\dot{v}| \le L_i$, a forward envelope is $v_0 - L_i s \le v(s) \le v_0 + L_i s$. Substituting these linear bounds into Equation (16) gives

$$y_f^{\pm}(s) = v_0 + (y_0 - v_0)e^{-s/T_A} \pm L_i\left[s - T_A\left(1 - e^{-s/T_A}\right)\right]. \tag{20}$$

The lower expression has no interior minimum: any interior stationary point can only be a maximum. Thus, its minimum is at one of the endpoints, and the completion test in Equation (18) remains sufficient after replacing y^- by y_f^-. The upper value at expiry similarly provides a sufficient reset test. Conservative slopes may leave many decisions unresolved; no claim of complete or accelerated protection prediction is made.

A slope bound follows from the invariant current disk and the phase equation. Within a fixed topology and source interval, one suitable bound is

$$B_I = \frac{2I_{max}}{T_I} + I_{max}k_{\mathrm{PLL}}V_{max}, L_i = \left(|Z_g|\sum_j s_j b_j + |Z_i|b_i\right)B_I. \tag{21}$$

where $V_{max} = |E_g| + (|Z_g| + max_j|Z_j|)I_{max}$ bounds terminal magnitude for the retained network. The first term in B_I bounds current component motion and the second bounds rotation of the reference frame. All terms in L_i are known at the event; L_i is in per unit per second. This bound applies to the instantaneous withdrawal baseline and excludes discontinuous voltage changes, which must be handled as new interval boundaries. With finite interruption, residual currents and their interruption time constants must remain in the slope bound.

For comparison, numerical trajectories also supply tighter retrospective constant envelopes. Their sample extrema are widened by $L_i h/2$, where h is the output spacing, to account for the distance to the nearest sample on a fixed-topology interval. This padding concerns interpolation between samples; it is not a rigorous enclosure of ODE integration error. Step refinement and independent integration are therefore reported separately. The retrospective and forward conditions are distinguished throughout the numerical results.

3.3. Residual DC Energy After Blocking

In the baseline model, blocking withdraws AC current immediately, so $p_{aci} = 0$ afterward. With the source target zero and source exit constant T_b, Equation (8) can be integrated without numerical time stepping:

$$p_{si}(t_k + s) = p_{sb}e^{-s/T_b}, w_i(t_k + s) = w_b + \frac{T_b p_{sb}}{T_E}(1 - e^{-s/T_b}). \tag{22}$$

where $p_{sb} = p_{si}(t_k)$ and $w_b = w_i(t_k)$ are continuous values at blocking. For $p_{sb} \geq 0$, the DC voltage is nondecreasing after blocking. Within this source and energy model, the infinite time non-exceedance condition is

$$w_{i,\infty} = w_b + \frac{T_b p_{sb}}{T_E} \leq V_{DH}^2. \tag{23}$$

For $p_{sb} > 0$ and $w_b < V_{DH}^2$, the corresponding critical source exit time constant is

$$T_{b,\mathrm{crit}} = \frac{T_E\left(V_{DH}^2 - w_b\right)}{p_{sb}}. \tag{24}$$

Strict inequality $T_b < T_{b,\mathrm{crit}}$ provides positive voltage headroom. Equality approaches the hard limit asymptotically and has no strict headroom; it is not treated as a robust operating recommendation. If the source power is zero, the voltage remains at its blocking value. If the hard limit has already been exceeded at blocking, the case fails independently of the source exit constant.

When $T_b > T_{b,\mathrm{crit}}$, the time at which the DC voltage reaches the hard limit is

$$t_H = t_k - T_b \ln\left[1 - \frac{T_E\left(V_{DH}^2 - w_b\right)}{T_b p_{sb}}\right]. \tag{25}$$

A case can therefore pass a short observation window and still violate the limit later. This is an analytical consequence of the retained energy and source model. If current interruption has finite duration, the more general energy relation contains the residual AC transfer:

$$w_{i,\infty} = w_b + \frac{T_b p_{sb}}{T_E} - \frac{1}{T_E}\int_{t_k}^{\infty} p_{aci}(t)dt. \tag{26}$$

Equation (23) is exact only for instantaneous port withdrawal. A nonnegative total residual AC integral bounds the final energy only. To use the instantaneous withdrawal solution as an upper bound throughout the transient requires nonnegative cumulative AC transfer at every time; $p_{aci}(t) \geq 0$ is a sufficient condition. Otherwise the finite interruption case must be assessed from its time-domain voltage peak. The finite interruption time calculations retain this AC/DC power exchange rather than adding an unaccounted ideal energy sink.

4. Assessment by Bounded Protection Setting Interventions

This section connects the protection state conditions to measurable changes in disconnection outcomes. All comparisons hold the fault, initialized operating point, and nonintervened parameters fixed. The modified trajectories are integrated again, so their later protection measurements include the resulting network feedback. Complete setting combinations reveal effects that are absent from one-device comparisons, while fixed hard limits prevent protection avoidance from being equated with equipment safety.

4.1. Intervention Set and Conditional Outcomes

Let $A \subseteq \{1,\ldots,n\}$ identify the units whose soft AC threshold is changed to the specified diagnostic value η'_A. The other AC thresholds, every DC threshold, and the hard limit, current limit, and source control parameters remain fixed. The setting is

$$\eta_{Ai}^{A} = \begin{cases} \eta'_A, & i \in A, \\ \eta_{Ai}, & i \notin A. \end{cases} \tag{27}$$

Each A generates its own trajectory Π_A. The intervention is a physical parameter change in the implemented protection function, not an instruction to keep a device connected

regardless of its remaining protections. Its role is diagnostic; the resulting threshold has not been validated as an acceptable field setting.

For each parameter vector in the finite set $\mathcal{G}$, the conditional collection of device outcomes at one operating point is

$$\mathcal{B}(c,\vartheta) = \{B_A(c,\vartheta) : A \subseteq \{1,\dots,n\}\}, B_A = \{i : t_i^A \le T\}. \tag{28}$$

where T is the observation horizon. This is a complete enumeration of the specified finite setting alternatives to the numerical resolution used. An absent subset is absent only from that finite collection; it is not proven unreachable under other thresholds, operating points, or controls. The empty subset is retained as a legitimate outcome.

4.2. Consequence Quantities and Equipment Limits

The device count and disconnected capacity fraction preserve different information:

$$N_A = \sum_i \mathbf{1}_{\{i\in B_A\}}, C_A = \sum_i s_i \mathbf{1}_{\{i\in B_A\}}. \tag{29}$$

where $\mathbf{1}$ is the indicator function. Device identities and first causes are also retained. Equal N_A does not imply equal disconnected capacity, equal power deficit, or an unchanged affected device. To include the transient deficit before and after each action, the assessment calculates

$$D_A = \int_0^T \sum_i s_i max\{0, p_{i0} - p_{aci}^A(t)\}dt. \tag{30}$$

The quantity D_A is in system per unit seconds. On a physical system base S_B in MW, $S_B D_A/3600$ is the corresponding deficit energy in MWh. No physical rating or occurrence frequency is assigned to the constructed benchmark.

Equipment limits are evaluated over the full trajectory, including the period after blocking:

$$H_A = max_{i,0\le t\le T}\left\{\frac{|V_i^A(t)|}{V_H}, \frac{\sqrt{w_i^A(t)}}{V_{DH}}, \frac{|I_i^A(t)|}{I_H}\right\}. \tag{31}$$

An outcome with $H_A > 1$ fails the declared hard-bound check regardless of its disconnection count. $H_A \le 1$ denotes non-exceedance of these specified limits within the horizon, not a complete converter stability guarantee. For an instantaneously blocked unit, Equation (23) additionally checks its infinite time source energy tail.

4.3. Device Changes and Interaction Among Local Settings

A unit exhibits channel migration if it disconnects under both compared settings but its first-cause identifier changes. The specific AC-to-DC case is

$$M_i(A,j) = \mathbf{1}_{\{r_i^A=\mathrm{AC}, r_i^{A\cup\{j\}}=\mathrm{DC}\}}, j \notin A. \tag{32}$$

The identifiers AC and DC in Equation (32) denote the soft functions; hard limit causes are recorded separately. An adjacent setting comparison also records the change in a peer's disconnection indicator:

$$F_{ij}(A) = \mathbf{1}_{\{i\in B_{A\cup\{j\}}\}} - \mathbf{1}_{\{i\in B_A\}}, i \ne j. \tag{33}$$

A positive value means that the peer disconnects only after unit j's threshold is changed. It identifies a conditional setting effect. Attributing that effect to removal of an earlier suppressive action additionally requires that unit j's action is altered and that the changed

trajectories support the proposed network mechanism. A negative value gives the opposite conditional direction. Neither value alone identifies an invariant causal edge for all operating conditions.

Single-device effects need not add because each setting change alters the trajectory on which the other protections operate. For any consequence $Y \in \{N,C,D\}$, the two-setting interaction relative to the original settings is

$$\Delta_{ij}Y = Y_{\{i,j\}} - Y_{\{i\}} - Y_{\{j\}} + Y_{\emptyset}. \tag{34}$$

For three units, the remaining third-order term is

$$\begin{aligned}\Delta_{123}Y = {} & Y_{\{1,2,3\}} - Y_{\{1,2\}} - Y_{\{1,3\}} - Y_{\{2,3\}} \\ & + Y_{\{1\}} + Y_{\{2\}} + Y_{\{3\}} - Y_{\emptyset}.\end{aligned} \tag{35}$$

These are deterministic finite differences of calculated outcomes, not statistical dependence measures. They satisfy the exact accounting identity

$$Y_{\{1,2,3\}} - Y_{\emptyset} = \sum_{i=1}^{3}(Y_{\{i\}} - Y_{\emptyset}) + \sum_{i<j}\Delta_{ij}Y + \Delta_{123}Y. \tag{36}$$

The sum of the three pair terms and the third-order term is therefore the error in adding isolated setting effects; individual nonzero terms can cancel. It does not prescribe the best setting, because acceptable protection detection and selectivity are additional engineering requirements outside the constructed intervention set.

4.4. Calculation Sequence

For each fault and parameter point, the calculation first solves the normal power balance and initializes the measurements and timers at equilibrium. It then integrates the continuous equations between fault and protection events, updates the connection state for each simultaneous action group, retains the states of all surviving devices, and checks the hard limits throughout the trajectory. Each of the specified threshold combinations is evaluated from the same initial state. Device sets, channel identifiers, event times, C_A, D_A, and H_A are stored together.

Pending AC timers are examined using Equations (18) and (20) only on intervals without another network or source change. A predicted completion is distinguished from the first-cause label if another channel acts first or simultaneously. Intervals that cannot be resolved retain the numerical trajectory result. At each blocking instant, the source power and DC energy states are recorded for Equations (23)–(25). Finally, matched interventions determine channel migration, peer device changes, and the interaction terms. This calculation produces a finite set of explicitly realized model trajectories, not a guarantee over an unspecified continuous uncertainty region.

5. Experimental Design and Numerical Verification

This section specifies the operating point, parameter sets, comparison models, and checks used to evaluate the assessment. The experiments separate reproduction of the retained equations from sensitivity to different physical or protection assumptions.

5.1. Operating Point and Fault Set

The normal common bus voltage is initialized to $1 + j0$ p.u. Each feeder's active power equation is solved on the normal voltage branch with zero initial local reactive power. The resulting external source is $E_{g0} = 0.988305661 - j0.254220987$ p.u., with magnitude 1.02047851 p.u.; it is not assigned unit magnitude independently of the load flow. Initial

DC voltages equal 1 p.u., source power equals AC power, and protection timers are zero. The total initial active power injection is 0.8002 p.u. on the system base.

The source disturbance begins at 0.20 s. During the fault, $E_g = 0.20E_{g0}e^{j20^\circ}$, and the source returns to E_{g0} at clearing. Thus, 0.20 is a relative source voltage multiplier, not an assertion that every terminal voltage is 0.20 p.u. Fault duration ranges from 80 to 222 ms in 2 ms increments, and K_q ranges from 2.40 to 3.70 in increments of 0.05. Their Cartesian product contains 1944 parameter points. Table 2 gives the unchanged electrical and protection parameters.

Table 2. Base case converter, network, and protection parameters.

Quantity	Value	Interpretation
s_1, s_2, s_3	0.34, 0.33, 0.33	Capacity weights
p_{10}, p_{20}, p_{30}	0.82, 0.78, 0.80 p.u.	Own converter bases
Z_g	$0.035 + j0.32$ p.u.	System base
R_1, R_2, R_3	0.015, 0.018, 0.021 p.u.	Own converter bases
X_1, X_2, X_3	0.065, 0.080, 0.095 p.u.	Own converter bases
T_I; k_{PLL}	3 ms; 65 s^{-1}	Current and phase response
T_v; T_A, T_D	20 ms; 2 ms, 2 ms	Control and relay filters
I_{max}; k_E	1.20 p.u.; 1.5	Current limit and energy feedback
T_E; T_s; T_b	250 ms; 120 ms; 8 ms	Energy and source response
v_f; Δv_f	1.10 p.u.; 0.16 p.u.	Source foldback
$\eta_{A1}, \eta_{A2}, \eta_{A3}$	1.180, 1.205, 1.230 p.u.	Original soft AC thresholds
$\eta_{D1}, \eta_{D2}, \eta_{D3}$	1.225, 1.230, 1.235 p.u.	Unchanged soft DC thresholds
d_A; d_D; η'_A	1 ms; 3 ms; 1.36 p.u.	Delays and diagnostic AC setting
V_H; V_{DH}; I_H	1.50; 1.32; 1.30 p.u.	Unchanged hard limits
T	1.20 s	Main observation horizon

The eight setting combinations span all subsets of the three units. The original settings, only unit 1 changed, and all units changed are also retained as a three-configuration comparison set. The principal mechanism points use fault duration and gain pairs of (200 ms, 3.70), (120 ms, 3.50), and (80 ms, 3.00), respectively. A no-action control uses (80 ms, 2.40); an aggravated case at (140 ms, 4.00) tests the hard AC boundary outside the main gain range. An earlier exploratory scan used a 4 ms AC delay and did not identify the targeted channel migration. The 1 ms study is therefore a mechanism-oriented design selected after exploration, not an independently sampled external validation set. The soft delays are much shorter than the overvoltage trip times that interconnection standards require of distributed resources, for example 0.16 s at 1.20 p.u. in IEEE Std 1547-2018 [31]; they were chosen to expose channel competition within a short post-fault overvoltage, not to represent a specific code requirement. To examine the dependence on this selection, Section 5.2 defines two pre-specified sensitivity sets whose settings and operating points were fixed by rule before evaluation, and Section 6.10 reports their results without adjustment. Because these sets belong to the same benchmark and were chosen by the authors, they are sensitivity cases rather than independent out-of-sample validation.

5.2. Model Comparisons and Sensitivity Cases

Three ablations isolate different errors in the protection representation. The zero-delay model acts when a filtered measurement first exceeds its threshold, with the corresponding explicit guard retained. The timer reset model incorrectly resets all surviving timers after another unit disconnects, while retaining their measurement filters. The DC channel omission model removes only the soft DC action and retains all hard limits. All three otherwise use the same converter and network equations as the reference. A severe disconnection

outcome is defined for this comparison as $N \geq 2$. Missed and additional severe outcomes are counted against the same-step full model; they are deterministic classification counts, not estimated risk rates. Because this classification depends on the chosen count threshold, the comparison counts are also reported for $N \geq 1$ and $N = 3$.

A fourth comparison model represents the conventional fixed-topology relay evaluation. The trajectory is computed once with every unit kept connected, and the protective functions of each unit, including their filters, timers, and hard limits, are evaluated on that trajectory to predict the unit's disconnection and first cause. The predicted outage set is therefore obtained without the electrical feedback of any disconnection on the remaining units, which is the simplification described in Section 1.2. Its comparison with the full model on the same grid quantifies the consequence of that omission within the retained equations. Because both evaluations share the converter, network, and relay models, the comparison is a logical necessity check: it shows which differences follow necessarily from omitting the feedback, but it is not external validation of the device sets predicted by the full model or of its feedback mechanism, which would require EMT simulation or protection coordination studies with measured relay characteristics.

Parameter sensitivity varies one quantity at a time: X_g by ±10%, T_I and T_A by factors of 0.5 and 2, T_E by ±10%, T_s by factors of 0.5 and 2, and fault phase to 0° and 40°. The 12 settings are evaluated at each of the three mechanism points and three threshold configurations, giving 108 runs. This experiment tests local dependence on modeling choices rather than an uncertainty distribution.

To test instantaneous current withdrawal, a further averaged model retains continuous terminal current after the trip latch. Once blocked, its current components satisfy

$$T_{\text{int}}\dot{i}_{di} = -i_{di},\ T_{\text{int}}\dot{i}_{qi} = -i_{qi},\ I_i = \left(i_{di} - ji_{qi}\right)e^{j\theta_i}. \tag{37}$$

where T_{int} is 0.5, 1, or 3 ms. The phase and capacitor energy equations continue, and p_{aci} is calculated from the resulting terminal current. This is a specified finite interruption time law with consistent port-power accounting; it is not a semiconductor commutation circuit or an independently validated hardware model. The zero-duration case uses the original instantaneous withdrawal, not a zero denominator in Equation (37).

Three further model variations are evaluated on the complete grid with all eight setting combinations, so that every count of Section 6.1 can be compared under each assumption. The first replaces the first-order phase model by a synchronous reference frame PLL with a proportional–integral regulator,

$$\dot{\theta}_i = k_p \Im\left\{V_i e^{-j\theta_i}\right\} + k_i \xi_i,\ \dot{\xi}_i = \Im\left\{V_i e^{-j\theta_i}\right\}. \tag{38}$$

where ξ_i is the integrator state, initialized at zero at the synchronized operating point. Three gain pairs are used: $k_p = 65\ s^{-1}$ with $k_i = 1056.25\ s^{-2}$, which gives a damping ratio of 1.0 at unit voltage; $k_p = 65\ s^{-1}$ with $k_i = 2112.5\ s^{-2}$, which gives a damping ratio of 0.707; and $k_p = 130\ s^{-1}$ with $k_i = 4225\ s^{-2}$, which gives a damping ratio of 1.0 with twice the natural frequency. The proportional gain of the first two pairs equals the first-order gain k_{PLL}. The second variation changes the control voltage floor in Equation (4) from 0.05 to 0.02, 0.20, and 0.60 p.u. The third applies the finite interruption law of Equation (37) with T_{int} of 1 and 3 ms to every grid point rather than to the three mechanism points only.

Two pre-specified sensitivity sets examine the mechanisms under settings and operating points that were not used in the exploratory selection. Their parameters were fixed by rule before any evaluation and were not adjusted afterwards. The setting-shift set raises every soft AC threshold and the diagnostic setting by 0.01 p.u., to 1.19, 1.215, 1.24, and 1.37 p.u.; changes the source depression to 0.25, the phase change to 15°, and the grid reactance to 0.30 p.u.; and keeps every other quantity. The delay set doubles the AC delay

to 2 ms and raises the DC delay to 5 ms with every other quantity unchanged. Both sets use the same 1944-point grid and all eight setting combinations. Because they were chosen by the authors within the same benchmark, they test whether the mechanisms persist within the retained model; they do not provide independent out-of-sample validation.

Repeated disturbances examine whether timer reset and timer hold can be interchanged. Two 80 ms source depressions begin at 0.20 and 0.65 s, with the same source multiplier and phase change. The ten combinations use gains of 3.0 and 3.5 and AC delays of 2, 4, 8, 12, and 20 ms; each is evaluated under both rules. The hold variant retains accumulated exceedance duration between separated episodes; the baseline resets it. Hard limits and the DC channel remain active (Table 3).

Table 3. Numerical studies and their distinct purposes.

Study	Evaluations	Purpose
Complete AC setting combinations	1944 × 8 = 15,552	Device, channel, and joint-setting effects
Adjacent setting comparisons	1944 × 12 = 23,328 pairs	Effect of one additional local change
Fine protection model comparison	1944 × 3 × 4 = 23,328	Full model and three ablations
Conditional AC timer checks	144 trajectories	Pending-timer inequalities and unresolved cases
Residual source energy cases	9 source exit constants	Analytical boundary and delayed violation
Independent original-case check	9 trajectories plus local interventions	Continuous event numerical verification
Parameter sensitivity	108 trajectories	Dependence on six parameter groups
Interruption time sensitivity	36 trajectories plus refinement	Dependence on current withdrawal dynamics
Repeated disturbance memory	20 trajectories plus refinement	Reset versus hold semantics
Targeted resolution and hard-boundary checks	1844 and 112 trajectories	Switching boundary and peak sensitivity
Fixed-topology relay evaluation	1944 × 3 = 5832	Conventional evaluation without network feedback
Full-grid model variations	8 × 15,552 = 124,416	Synchronization model, control voltage floor, interruption time
Pre-specified sensitivity sets	2 × 15,552 = 31,104	Persistence of the mechanisms under pre-specified settings and operating points

These counts identify separate experiments and are not summed as independent statistical observations.

5.3. Solvers, Event Resolution, and Conservation Checks

The primary calculations use midpoint Runge–Kutta integration with endpoint guard evaluation. The complete setting enumeration and primary protection ablation comparison use 62.5 µs. A 250 µs calculation is retained for resolution comparison, and every ablation is compared with a full-model reference at the same step. Selected event cases use 500, 250, 125, 62.5, 31.25, and 15.625 µs as applicable. Fault boundaries are aligned with the step grid. Event order within one time step is reported as unresolved or simultaneous at that resolution rather than interpreted as a causal ordering. Local guard sampling is step-sized, but accumulated changes in a hybrid trajectory can produce event-time differences greater than one step.

The network residual follows Equation (3). The DC energy residual compares $T_E[w_i(T) - w_i(0)]$ with the integrated input–output power difference. Initial no-fault and perturbed-no-fault checks establish that the retained normal operating point does not drift into a

protection action. Conservation residuals test implementation consistency. They neither compensate for missing circuit dynamics nor establish field model accuracy.

5.4. Implementation and Verification Procedure

The calculation for one fault, operating point, and setting combination proceeds in five steps. First, the normal operating point is solved from each feeder's power equation, the external source voltage is computed from the resulting weighted currents, and all measurements and timers are initialized at equilibrium. Second, the continuous states of all units are advanced by one midpoint step; the algebraic network is solved at the start, midpoint, and end of the step with the current connection states. Third, at the end of the step, the guards of each connected unit are evaluated: the AC and DC timers are increased by the step if their filtered measurements exceed their thresholds and are otherwise reset; a soft action is registered when a timer reaches its delay, and a hard action is registered when an instantaneous limit is exceeded. Fourth, every unit whose action is registered in that step is blocked at the same instant: its connection state is set to zero, its first cause and action time are stored, and its current references and source target are set to zero, while all continuous states of all units, including the timer ages of the surviving units, are carried unchanged into the next step. Fifth, the hard limit index, the deficit integral, and the energy residual are accumulated over the horizon. The primary implementation is a Python (version 3.11.9) program compiled with Numba; the complete grid, the eight setting combinations, the protection model comparisons, the model variations, and the parameter, interruption time, and repeated disturbance studies of Section 6.8, for which the program also provides the timer-hold rule and a second source depression, are evaluated by the same program with different parameter sets. All trajectories reported in Section 6 are computed with this program, except the continuous event values identified as such, which come from the verification implementation described next.

The procedure is verified in three ways. First, a separately written SciPy implementation shares no code with the primary program: it initializes each feeder from the analytic root of its power equation, integrates between events with DOP853 at a relative tolerance of 10^{-9}, an absolute tolerance of 2×10^{-11}, and a maximum step of 0.5 ms, and locates guard crossings, timer expiries, and hard limit contacts as continuous events, so that event times are not quantized by a step; its agreement with the primary program, tests the equations against step quantization and event handling. Second, step refinement of the midpoint integration (Sections 5.3 and 6.8) tests the dependence of the event sequences on the resolution. Third, the network and DC energy balance residuals of Section 5.3 and the closed-form relations of Equations (14) and (22) test the consistency of the implemented equations. None of these checks tests the physical adequacy of the retained equations.

6. Results

The results connect the finite collection of action trajectories with the network, timer, and energy conditions derived above. Full-grid outcomes establish the frequency of each behavior within the specified deterministic set; representative trajectories explain the mechanism. Comparisons with reduced protection representations and altered interruption dynamics then identify which conclusions depend on retained state and model assumptions.

6.1. Complete Setting Combinations and Device-Specific Changes

The complete evaluation at 62.5 µs contains 15,552 trajectories, all of which are below the declared hard limits. The original AC settings produce at least one disconnection at 1224 of 1944 parameter points; changing all AC settings reduces this count to 261. Ten parameter points exhibit soft AC-to-soft DC migration in the matched original-versus-all

changed comparison. Changing only unit 1's AC setting reveals 269 points at which its original AC action suppresses a peer's disconnection; this count is a diagnostic observation of the averaged model under instantaneous current withdrawal, and Section 6.9 reports how it changes under an assumed finite interruption law. Within this particular intervention family, no opposite case is found in which unit 1's original AC action is necessary for a peer to disconnect.

The complete eight-setting set permits 12 directed single-setting comparisons per parameter point. Among the 23,328 resulting comparisons (Table 4), none increases the total disconnected unit count. Nevertheless, 830 comparisons produce a newly disconnected peer, 40 replace the modified unit's AC action with a DC action, and 183 increase the deficit integral. In all 830 peer-change comparisons, the modified unit itself changes from an AC disconnection to remaining connected. The largest deficit increase is 0.005962275 p.u. s. Thus, a nonincreasing unit count does not establish an unchanged affected-device set or a nonincreasing transient deficit.

Table 4. Outcomes of the complete setting evaluation at 62.5 µs.

Quantity	Count	Denominator or Scope
Trajectories violating a declared hard limit	0	15,552 trajectories
Original setting points with any disconnection	1224	1944 parameter points
All-changed points with any disconnection	261	1944 parameter points
AC-to-DC migration, original versus all changed	10	1944 parameter points
Suppression identified by the unit 1 comparison	269	1944 parameter points
Single-setting comparisons increasing unit count	0	23,328 comparisons
Single-setting comparisons creating a peer action	830	23,328 comparisons
Modified unit AC-to-DC changes	40	23,328 comparisons
Single-setting comparisons increasing deficit	183	23,328 comparisons

The absence of count increases is a structural property of this benchmark rather than a physical guarantee, and three features of the retained model produce it. First, a higher pick-up value can only shorten or remove the uninterrupted exceedance intervals of a given measured trajectory, so a definite time element with a raised threshold acts later or not at all; because the timer states do not enter the continuous dynamics, the two trajectories of a comparison coincide until the original AC action of the modified unit. Accordingly, the 12,395 comparisons in which that unit was not originally disconnected by its AC function give identical outcomes, and in the other 10,933, no unit that disconnected at or before the original action instant changes its action. Second, a disconnection relieves the remaining units: both current references of Equations (4) and (5) are nonnegative and the synchronization angle follows the terminal voltage, so the cross term of Equation (15) dominates, and at all 12,070 disconnection instants with surviving units in the 15,552 trajectories the terminal voltage of every surviving unit falls, by 0.054 to 0.229 p.u. Because the retained relay functions are overvoltage functions, the loss of this relief when a unit stays connected tends to add peer actions rather than remove them, and no comparison removes a peer's disconnection. Third, the substitution is one-for-one: when the modified unit remains connected (10,857 comparisons), at most one peer disconnects in its place (830 comparisons), and the withdrawal of that peer relieves the third unit as the original action did; when the modified unit instead acts later through its DC function (40 comparisons) or through its AC function at the diagnostic threshold (36 comparisons), it does so within 2.6 ms and no peer outcome changes. The count can therefore change by -1 or 0 but not by $+1$. Each feature can fail in other systems: a disconnection that raises the remaining voltages; undervoltage functions acting during the fault, where the withdrawal of reactive support deepens the depression; or units of very different ratings could turn a less sensitive AC setting into an

additional disconnection. The absence of count increases is therefore a property of the retained model and of the evaluated grid.

All eight terminal device subsets occur somewhere in the evaluated parameter set. At 461 points, the eight setting alternatives generate all eight subsets; at 749 points, every alternative gives the same subset. Summing the distinct subsets separately at each point gives 7331 conditional outcomes. These observations do not support a universal assertion that particular outage combinations are impossible. They instead show why a subset must be associated with its fault, operating point, and protection settings. Because every alternative was simulated, this enumeration is not a demonstrated reduction in computation time.

Figure 2 contrasts the original and jointly changed AC settings and locates the channel migration and peer device change regions. In panels (a) and (b), the color scale gives the number of disconnected units at each of the 1944 parameter points, and the lightest cells are evaluated points at which no unit disconnects within the horizon. In panels (c) and (d), every evaluated point is drawn in gray, and the colored squares mark the points at which the indicated effect occurs: an AC-to-DC change in a unit's first cause between the original and the all-changed settings in (c), and a peer disconnection that appears only when unit 1's setting is changed in (d). A broad improvement in disconnection count can coexist with a local change in the affected device or channel. The parameter maps do not assign equal physical likelihood to the plotted cells, and the counts are not estimates of occurrence probabilities.

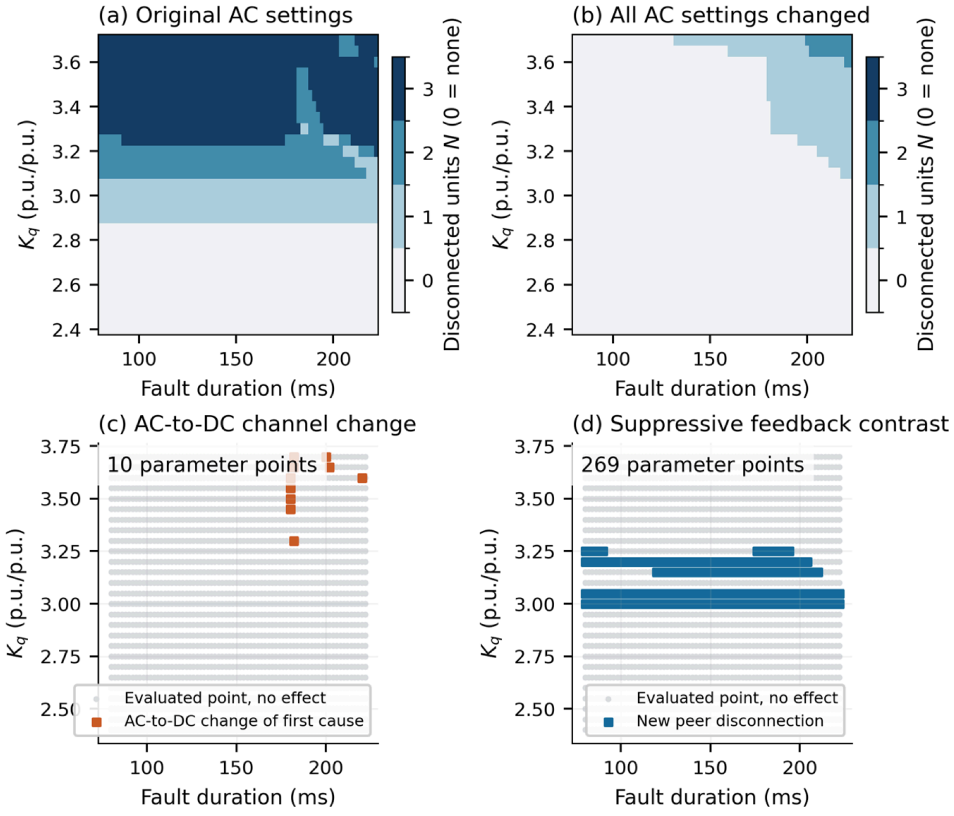


Figure 2. Full parameter evaluation at 62.5 µs: (**a**) number of disconnected units with the original AC settings; (**b**) the same number with all AC settings changed; the color scale gives the count, and the lightest cells are points without any disconnection; (**c**) the 10 points with an AC-to-DC change in a unit's first cause under the matched all-unit change; and (**d**) the 269 points with a new peer disconnection when only unit 1's AC setting is changed. In (**c**,**d**), gray dots are evaluated points without the effect and colored squares are points with it.

6.2. AC-to-DC Protection Channel Migration

At a 200 ms fault duration and K_q = 3.70, unit 1 first disconnects through its DC protection; units 2 and 3 subsequently disconnect through their AC protections. Changing only unit 2's soft AC threshold from 1.205 to 1.36 p.u. removes its AC action, but the same unit then completes its DC timer. Independent continuous event calculations place its AC action at 0.404223549 s in the original case and its DC action at 0.406743937 s after the local change. The intervention delays the unit's disconnection by approximately 2.52 ms and changes its initiating channel; it does not keep the unit connected.

Figure 3 shows the two protection measurements, connection state, and system active power. All three units disconnect in both cases. At 62.5 µs, the deficit integral changes from 0.770809301 to 0.770228160 p.u. s, a reduction of only 0.000581140 p.u. s. The modified trajectory remains below the declared hard limits, with peak AC voltage 1.389309 p.u., peak DC voltage 1.237175 p.u., and current limited to 1.20 p.u. Removing the AC action therefore changes the protection explanation much more than the final system consequence.

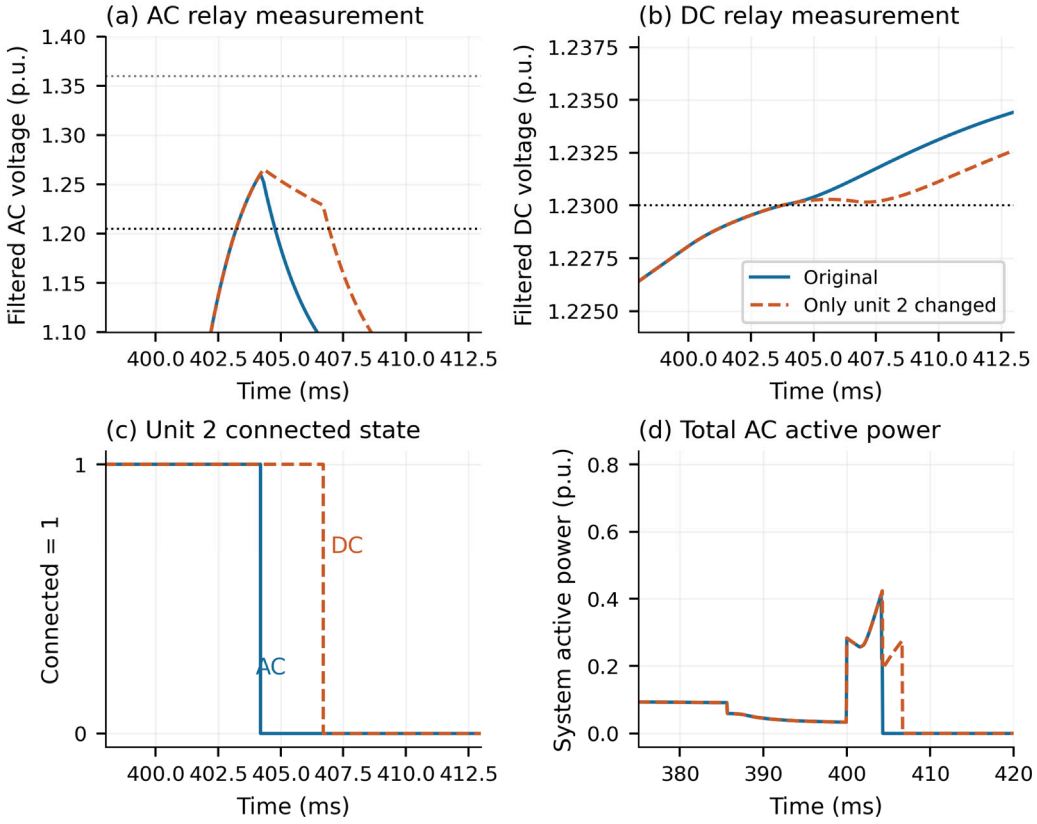


Figure 3. Channel competition for unit 2 under the original settings and a change to only its AC threshold: (**a**) filtered AC voltage; (**b**) filtered DC voltage; (**c**) connection state; and (**d**) system active power. The trajectories use a 62.5 µs step; the action times quoted in the text are independently refined.

When all three AC thresholds are changed at the same point, unit 3 remains connected, but units 1 and 2 still disconnect through DC protection. Thus, the local and joint interventions give different device sets. Comparing AC operation alone would misclassify both outcomes as complete protection avoidance. The retained DC measurement and energy state are what distinguish delayed channel replacement from continued connection.

6.3. Common Disturbance and Suppressive Network Feedback

The 120 ms, K_q = 3.50 case illustrates common disturbance exposure. At 62.5 µs, the first sampled AC guard crossings occur at 0.3224375, 0.3225000, and 0.3226875 s. All

precede the first disconnection at 0.3233750 s. The actions occur at 0.3233750, 0.3234375, and 0.3236250 s. Guard ordering alone does not establish independence, because an earlier action might still determine whether a later timer survives. The setting comparisons provide the necessary additional check: retaining each target's original AC threshold while changing the other two leaves the target's AC disconnection in place and prevents the peers from disconnecting. Each target action therefore remains possible without the other two actions in these matched interventions.

The first row of Figure 4 shows these guard histories and target-only outcomes. The 0.1875 ms difference between the last two sampled action times is not sufficient evidence of a directed cascade. The target's filtered voltage and timer age already contain the disturbance history before any peer disconnects.

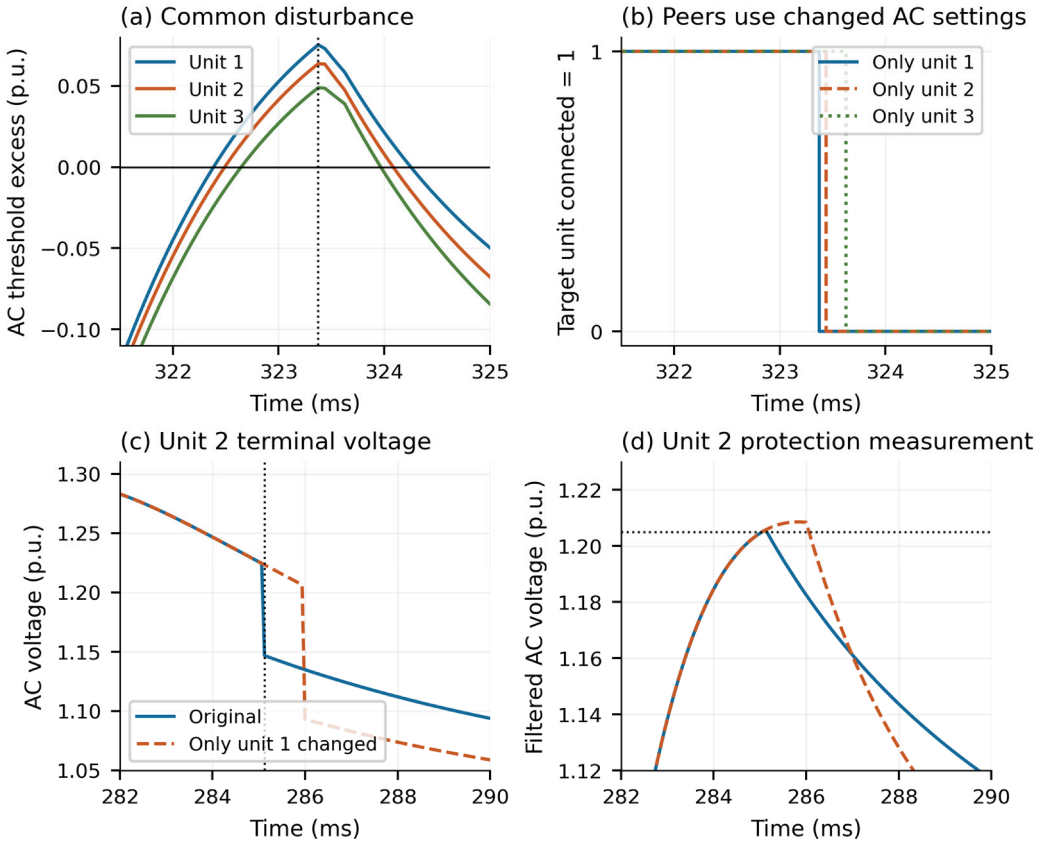


Figure 4. Common disturbance and suppressive feedback: (**a**) AC measurement excesses before the first action; (**b**) persistence of each target action when peer AC settings are changed; (**c**) unit 2 terminal voltage with and without the original unit 1 action; and (**d**) the resulting unit 2 protection measurement. The trajectories use a 62.5 µs step.

The 80 ms, $K_q = 3.00$ case exhibits a different mechanism. With the original settings, only unit 1 disconnects. Changing only its AC threshold leaves unit 1 connected but causes unit 2 to disconnect; changing all thresholds produces no disconnection within the observation horizon. At the original unit 1 action, the current is $I_1 = 1.054401644 - j0.499822334$ p.u. Equation (14) gives a peer voltage change of $-0.066928049 - j0.108771013$ p.u. Recalculation at the same continuous state changes unit 2's voltage magnitude from 1.223155422 to 1.146674706 p.u., which is a reduction of 0.076480716 p.u. The complex voltage jump relation is satisfied to 1.6×10^{-16} p.u. in this calculation.

The second row of Figure 4 shows why that electrical change matters. Unit 2's filtered AC voltage falls below its threshold before its residual timer duration expires. When unit 1's action is avoided, this voltage reduction is absent and unit 2 completes its timer. The

disconnected capacity fraction changes from 0.34 to 0.33 even though the disconnected unit count remains one. The effect is suppressive under this stated intervention and current withdrawal model. It is not a general rule that disconnection improves the condition of neighboring converters.

6.4. Pending Timers and the Effect of Retained Measurement History

The conditional timer study contains 144 trajectories and 72 eligible pending AC episodes after a network action. At 62.5 µs, the retrospective input-envelope inequalities classify 64 completions and eight resets, with no disagreement against the corresponding integrated trajectories. The same counts and outcomes remain at 31.25 µs. In 24 of the completion episodes, the raw terminal magnitude remains below the AC threshold throughout the residual timer interval. The protective function nevertheless completes because the filtered measurement is still above threshold and the timer retains a nonzero age. This is the measurement lag of Equation (19): the disconnection of a peer lowers the terminal voltage below the threshold at once, but the relay's measured quantity follows with the time constant T_A, and a timer with less remaining duration than that lag expires first. In relay terms, the overvoltage element has already picked up, its definite time delay is almost complete, and the drop-out of the measured quantity arrives too late to reset it. The classifications themselves come from the integrated trajectories; the inequalities explain them.

For the feedback case at 62.5 µs, unit 2 has accumulated 0.125 ms when unit 1 disconnects, leaving 0.875 ms. Its initial filtered measurement is 1.205741 p.u., which is slightly above the 1.205 p.u. threshold. A padded upper terminal voltage envelope of 1.155130 p.u. gives an upper measurement at expiry of 1.187807 p.u. Equation (18) therefore guarantees reset of that episode under the retained input envelope. By contrast, for the 80 ms, $K_q = 3.30$ case, unit 3 retains a 0.6875 ms age after a preceding action. Its terminal voltage remains below 1.23 p.u. during the remaining 0.3125 ms, yet the filtered lower bound at expiry is 1.231855 p.u.; the timer study produces decisions for the 72 pending AC episodes identified in the 144 trajectories (Table 5).

Table 5. Conditional timer decisions for the 72 pending AC episodes identified in the 144 trajectories of the timer study, which provided the denominators for each column. The reference for each episode is the outcome of its directly integrated trajectory; a contradiction would be a decision opposite 08:23:16to that outcome.

Decision Method	Completed Episodes Identified	Reset Episodes Identified	Unresolved	Contradictions
Retrospective constant envelope, 62.5 µs	64	8	0	0
Forward slope envelope, 62.5 µs	63	0	9	0
Retrospective constant envelope, 31.25 µs	64	8	0	0
Forward slope envelope, 31.25 µs	64	0	8	0

The forward condition uses only the event state and Equation (21). Its conservative slope fails to identify the reset episodes and therefore returns unresolved results. This is the intended behavior of a sufficient test. The tighter retrospective calculation uses future interval extrema and cannot be presented as a forward prediction. Both comparisons are numerical tests of the stated conditional inequalities; neither establishes a rigorous ODE-error enclosure or a complete event sequence guarantee.

Figure 5 shows the decision margins and their sensitivity to widening the voltage envelope. Widening each side of the input envelope by δ moves the bounds at expiry by $\delta\left(1 - e^{-\rho/T_A}\right)$, as Equation (17) shows, so a decision survives only while its margin exceeds this shift. The unresolved fraction in panel (b) therefore grows with the envelope

width because the episodes with the smallest margins lose their decision first. The eight reset episodes have margins between 0.012 and 0.017 p.u. with remaining durations of 0.75–0.875 ms, for which the factor $1 - e^{-\rho/T_A}$ is 0.31–0.35: a widening of 0.05 p.u. moves their bounds by 0.016–0.018 p.u. and removes all eight reset decisions, whereas 0.025 p.u. moves them by at most 0.009 p.u. and removes only the completion with the smallest margin, 0.0019 p.u. at 0.31 ms remaining. Adding 0.025 p.u. to each side of the 62.5 µs retrospective envelope thus leaves one episode unresolved, and 0.05 p.u. leaves nine unresolved, including all eight reset episodes. No opposite decision is introduced. For practical use, the forward test can confirm a pending completion from the event state alone when the margin is large, but resolving the marginal episodes, which are precisely the reset cases produced by network relief, requires the terminal voltage over the residual interval to be known within roughly 0.01–0.02 p.u. Retaining an unresolved category prevents an imprecise voltage estimate from being interpreted as either confirmed completion or confirmed reset.

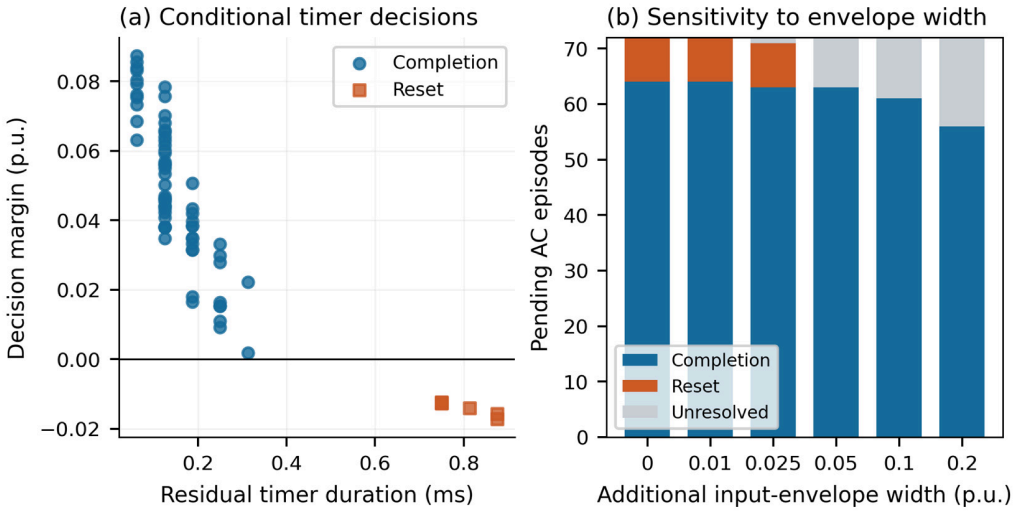


Figure 5. Conditional timer evaluation: (**a**) retained or reset episodes plotted by remaining duration and decision margin; (**b**) loss of resolution when the retrospective voltage envelopes are widened. The base calculation uses 62.5 µs samples and includes the between-sample slope allowance.

6.5. Residual Source Energy Boundary

For unit 1 in the channel migration case, continuous event integration gives a blocking time of 0.385724324 s, $w_b = 1.512122022$, and $p_{sb} = 0.579947449$ p.u. Equation (24) therefore gives $T_{b,\mathrm{crit}} = 99.266743$ ms. The nominal 8 ms source exit is well below this model boundary. A protection model that sets p_{si} immediately to zero would remove the entire term $T_b p_{sb}/T_E$ and would miss the dependence on source exit dynamics.

The numerical tail cases in Figure 6 and Table 6 use the blocking state produced at 62.5 µs, whose own exact boundary is 99.280299 ms. The 0.013556 ms difference from the continuous event value arises from the slightly different blocking states. Each numerical trace is compared with Equation (22) using its actual blocking state, so the comparison does not mix these two initial conditions. The maximum voltage discrepancy over the nine tail cases is 2.85×10^{-8} p.u.

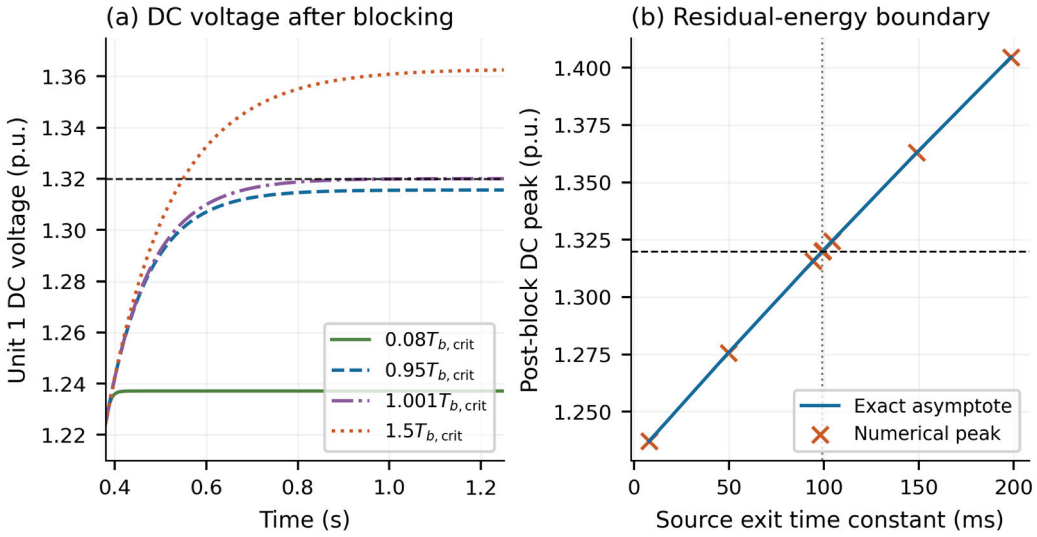


Figure 6. Residual DC source energy after blocking: (**a**) DC voltage trajectories for several source exit constants; (**b**) exact asymptotic voltage and numerical peaks. The dashed horizontal line is the 1.32 p.u. hard DC limit, and the vertical line is the boundary associated with the sampled blocking state.

Table 6. Residual energy checks for unit 1 using the 62.5 µs blocking state.

Source Exit Constant (ms)	Exact Asymptotic DC Voltage (p.u.)	Predicted Hard Limit Time (s)	Numerical First Exceedance (s)
7.942424	1.237121	No exceedance	No exceedance
49.640149	1.275625	No exceedance	No exceedance
94.316284	1.315630	No exceedance	No exceedance
99.181018	1.319913	No exceedance	No exceedance
99.379579	1.320087	1.072277	1.072313
104.244314	1.324356	0.703062	0.703063
148.920448	1.362931	0.549293	0.549313

The 99.379579 ms case is particularly informative. The device has already disconnected at approximately 0.386 s, while its DC voltage reaches the hard limit only at 1.072277 s. Its disconnection cause is unchanged; its post-action energy outcome is different. At the exact critical constant, the voltage approaches 1.32 p.u. without positive headroom. The criterion therefore supplies an energy interpretation of the source exit requirement instead of treating the absence of further AC injection as a safety result.

6.6. Nonadditive Effects of Local Protection Changes

At 62.5 µs, the all-unit count predicted by adding the three isolated setting effects differs from the actual all-unit result at 326 of 1944 points. The discrepancy ranges from two fewer units to one more unit than the additive prediction. The corresponding deficit discrepancy is nonzero at 749 points, using a numerical tolerance of 10^{-8} p.u. s, and ranges from −0.483417 to +0.227636798 p.u. s. Nonzero pairwise count terms occur at 249, 125, and 37 points for pairs (1,2), (1,3), and (2,3), respectively; the third-order count term is nonzero at 141 points. The complete expansion in Equation (36) reconstructs every count exactly and every deficit to within 2.22×10^{-16} p.u. s.

Table 7 gives two contrasting cases. Case A uses an 80 ms fault and a gain of 3.25; Case B uses a 132 ms fault and a gain of 3.70. All 16 trajectories satisfy the declared hard limits, and their first-cause vectors agree with independently implemented continuous event integration.

Table 7. Complete setting combinations for two nonadditive cases at 62.5 µs.

Units with Changed AC Threshold	Case A Unit Count	Case A Deficit (p.u. s)	Case B Unit Count	Case B Deficit (p.u. s)
None	2	0.534799	3	0.775892
1	2	0.521091	2	0.534779
2	2	0.540761	2	0.553289
1, 2	1	0.285345	1	0.312174
3	2	0.534799	2	0.547598
1, 3	1	0.279383	1	0.306490
2, 3	1	0.299052	1	0.324995
1, 2, 3	0	0.043637	1	0.311519

These comparisons establish a practical limitation of adding separate setting benefits. At one point, every single change leaves two units disconnected, while the joint change keeps all three converters connected. At another, each single change reduces the count by one, but their sum incorrectly predicts that no unit will disconnect. The state-dependent network response explains why isolated effects need not be additive. Equations (34)–(36) quantify this behavior without assigning a universal beneficial or adverse sign to any local setting.

6.7. Consequences of Omitting Timing or DC Protection

The fine comparison contains 5832 trajectories for each protection representation, all at 62.5 µs. The full model has 1770 severe outcomes; a severe outcome is defined as two or more disconnected units. Table 8 reports errors relative to that same-step reference. Zero-delay protection misses 434 severe outcomes; resetting surviving timers after another action misses 182 severe outcomes. Removing the soft DC function misses 183 cases with any disconnection and also produces 57 activations of the AC hard boundary.

Table 8. Protection model comparisons against the full model at the same 62.5 µs step on the 5832 trajectories of the three original setting configurations (1944 points × 3). The full model is the computational reference: a different device set is a different terminal set of disconnected units; a missed severe outcome is a reference outcome with $N \geq 2$ that the comparison model classifies below two; an additional severe outcome is the converse.

Protection Representation	Different Device Set	Missed Severe Outcomes	Additional Severe Outcomes	AC Hard-Boundary Activations	Maximum Deficit Error (p.u. s)
Full model	0	0	0	0	0
Zero soft delays	1119	434	12	0	0.470986
Reset surviving timers	253	182	0	0	0.241610
Omit soft DC action	512	25	35	57	0.422889
Fixed-topology relay evaluation	613	2	290	57	Not applicable

Earlier action is not uniformly conservative for a multi-converter study. In the zero-delay model, early withdrawal of one injection can remove the electrical stimulus that would otherwise complete another unit's timer. It consequently predicts fewer severe outcomes even though its local relays are faster. The timer reset ablation directly erases a physical state of surviving devices; its errors quantify the consequence of that deletion rather than an alternative implementable setting. Omitting DC protection changes both protection causes and trajectories. Its 57 hard-boundary activations are retained as failed soft-protection outcomes, not reinterpreted as successful avoidance. Of these, 54 occur at the algebraic voltage jump on fault clearing; three occur during subsequent continuous motion, where the fixed-step exceedance contains a numerical overshoot component.

The fixed-topology relay evaluation, which applies the same protective functions to the trajectory computed without any disconnection, gives a different device set in 613 of

the 5832 runs. It predicts more disconnected units than the full model in 610 runs and fewer in two, and in 30 further runs the device set agrees but a first cause differs. Because no unit is ever removed from its trajectory, this evaluation cannot represent the relief that a first disconnection gives to the remaining units: it reports none of the 269 suppression points, classifies 290 outcomes as severe that the full model does not, and records the same 57 AC hard-boundary contacts at fault clearing as the DC omission model, contacts that the earlier soft actions of the full model prevent. Its prediction of whether any unit disconnects is, however, identical to that of the full model in every run. On this benchmark, the conventional evaluation is therefore conservative in the unit count but departs from the full model in which units disconnect, through which function, and whether a local setting change shifts the disconnection to a peer. Because the two evaluations share the same equations, these differences are logical consequences of omitting the feedback within the retained model; they show that the omission changes the predicted device sets, not that the device sets or the feedback mechanism of the full model are physically correct, which would require comparison with EMT simulations or recorded relay operations.

Figure 7 compares the two nonadditive setting examples with the ablation results. The severe-outcome detection proportions are 75.48% for zero delay, 89.72% for resetting surviving timers, and 98.59% for omitting soft DC action. The last proportion alone would hide the 183 missed any-disconnection cases, altered first causes, and hard-boundary activations. Reporting several consequence quantities is therefore necessary, even in this small system.

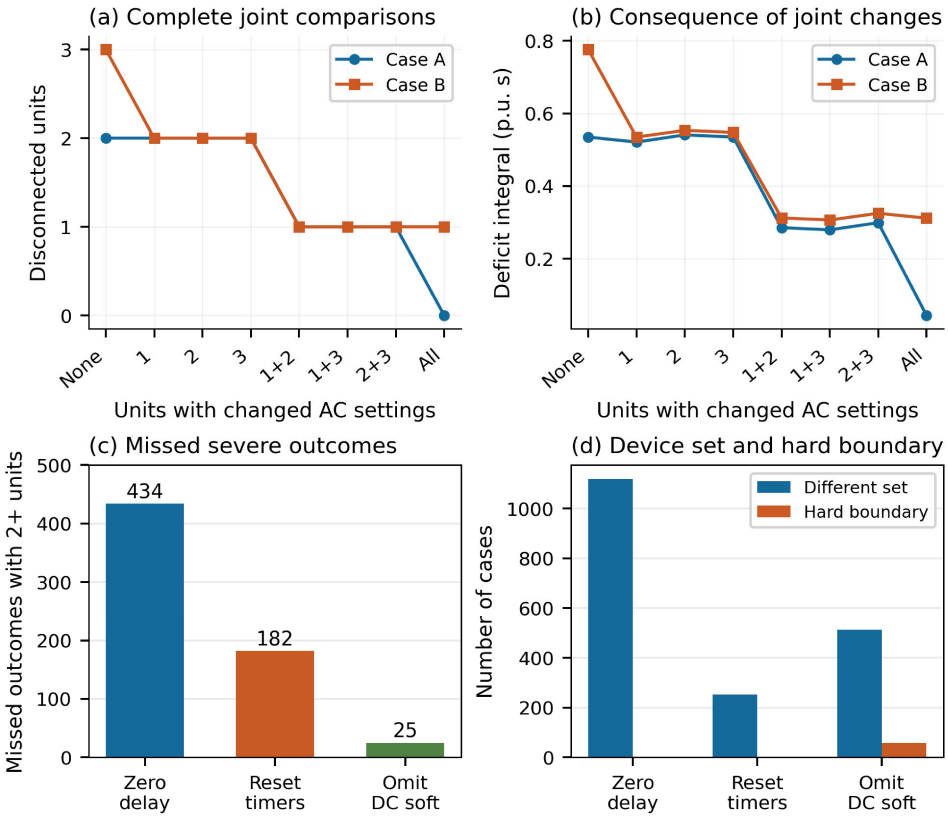


Figure 7. Joint-setting effects and protection model ablations: (**a**) disconnected unit counts for two complete eight-setting comparisons; (**b**) corresponding power deficit integrals; (**c**) severe outcomes missed by each ablation at 62.5 µs; and (**d**) different terminal device sets and hard-boundary activations.

The severe outcome classification is threshold-dependent. Table 9 repeats the comparison for three count thresholds. With $N \geq 1$, the zero-delay and timer reset models miss no outcome and only the DC omission model misses 183; with $N \geq 2$, the zero-delay model misses 434 of 1770; with $N = 3$, it misses 701 of 825 because its early actions remove the

stimulus that would otherwise disconnect the third unit, whereas the fixed-topology evaluation adds 358 outcomes with three units that the full model does not produce. The ranking of the comparison models therefore changes with the threshold, and a protection model comparison should report at least two thresholds together with the device-set agreement.

Table 9. Dependence of the comparison counts on the severe outcome threshold, on the same 5832 runs as Table 8. The full model has 2565 runs with $N \geq 1$, 1770 with $N \geq 2$, and 825 with $N = 3$; missed and additional counts are relative to it.

Comparison Model	Different Device Set	Missed $N \geq 1$	Additional $N \geq 1$	Missed $N \geq 2$	Additional $N \geq 2$	Missed $N = 3$	Additional $N = 3$
Zero soft delays	1119	0	11	434	12	701	4
Reset surviving timers	253	0	0	182	0	57	14
Omit soft DC action	512	183	0	25	35	172	37
Fixed-topology relay evaluation	613	0	0	2	290	0	358

6.8. Numerical Verification and Sensitivity to Model Assumptions

Independent continuous event integration reproduces all nine original representative first-cause vectors. Relative to the 250 µs midpoint trajectories, its maximum event-time difference is 0.240025 ms; peak AC and DC voltage differences are 1.769×10^{-4} and 1.964×10^{-4} p.u. The two eight-setting nonadditivity examples also retain all 16 first-cause vectors under continuous event verification and 62.5 µs integration. These selected agreements do not imply that every parameter point is insensitive to resolution: 117 of the 15,552 complete setting cause vectors change between 250 and 62.5 µs.

Indeed, refining the three original threshold configurations from 250 to 62.5 µs changes 64 of 5832 device sets and 34 severe outcome classifications. The ablation counts also change: zero-delay missed severe outcomes increase from 351 to 434, and timer reset misses increase from 156 to 182. The fine counts are therefore used in Table 8. Near a switching boundary, a small event-time change can alter later trajectories; a narrow parameter-bisection interval alone does not establish numerical convergence.

A targeted refinement at 31.25 µs evaluates 1844 trajectories across 614 parameter points, which were selected from prior resolution changes, adjacent grid points, matched references, and large ablation errors. Forty-eight first-cause vectors change relative to 62.5 µs: 34 in the full model, eight with zero delay, five with timer reset, and one with DC omission. Independent continuous event calculations agree with the 31.25 µs result in 46 cases and with the 62.5 µs result in two. The remaining two timer reset cases require 3.90625 and 7.8125 µs, respectively, to recover the continuous event action set. This nonmonotone local convergence prevents interpreting a single step reduction as a proof of correctness. The selected cases do not provide a population accuracy estimate; the full-grid tables remain explicitly resolution-specific observations.

A separate near-hard-boundary check examines 112 cases with 31.25 µs integration and independent dense-output peak maximization within each unchanged-mode interval. All action vectors agree and no hard contact is found. The largest optimized AC peak is 1.499995655 p.u., leaving only 4.345×10^{-6} p.u. below the 1.50 p.u. limit. Nominal non-exceedance in this set therefore provides almost no tolerance to parameter or model error and is not a robust safety margin (Table 10).

Table 10. Implementation and numerical verification results.

Comparison	Cases	First-Cause Agreement	Maximum Reported Discrepancy
Independent DOP853 versus 250 μs midpoint	9	9/9	0.240025 ms in action time
Complete setting mechanism examples, DOP853 versus 62.5 μs	16	16/16	0.053684 ms in action time
Source tail equation versus midpoint voltage	9	Not applicable	2.85×10^{-8} p.u.

The original full scan has a maximum DC energy balance residual of 1.29×10^{-13} p.u. s. A check using the finite-precision exported waveforms gives a maximum network power residual of 9.10×10^{-12} p.u. The new fine reference retains residuals of the same numerical order.

The parameter variations demonstrate the limits of transferring a representative pattern to other conditions. Table 11 reports the exact first-cause vector retention counts. Increasing T_E from 0.25 to 0.275 s in the migration case produces an AC hard limit action in three configurations. A larger capacitor energy time constant therefore does not guarantee a better combined AC/DC protection outcome: the changed energy trajectory also changes active power extraction and the timing of network withdrawal.

Table 11. Sensitivity of the three mechanism cases to the 12 individual parameter changes.

Mechanism Point	Configurations Retaining the Original Cause Vector	Parameter Settings Retaining All Three Vectors	Hard Limit Violations
Channel migration	19/36	2/12	3/36
Common disturbance	28/36	6/12	0/36
Suppressive feedback	21/36	4/12	0/36

Finite interruption time, represented by the first-order law of Equation (37), produces an especially direct qualification of the feedback interpretation. Across 27 nonzero-interruption configurations, 26 retain the instantaneous model's first-cause vectors. The exception is the original feedback case at 3 ms, where unit 2 now completes its AC timer. At 31.25 μs, the instantaneous and 3 ms cases have deficit integrals of 0.296836411 and 0.529920842 p.u. s, respectively; the latter disconnects units 1 and 2 at 0.285125 and 0.28603125 s. This is loss of the previously observed suppression, not sufficient evidence that the first disconnection positively caused the second. Section 6.9 extends this comparison to the full grid and shows that, under this law, the loss is the rule rather than the exception (Table 12).

The transition in the feedback case is step-sensitive. Bisection brackets the appearance of unit 2's action between 2.430664 and 2.431641 ms at 62.5 μs, between 2.571289 and 2.572266 ms at 31.25 μs, and between 2.568359 and 2.569336 ms at 15.625 μs. The supported interpretation is an approximately 2.57 ms conditional transition in this finite interruption model, not a hardware threshold known to the width of the final bisection interval.

Figure 8 shows the current withdrawal and memory effects. Reset and hold give identical outcomes in the 15 original single-disturbance configurations, but five of ten repeated disturbance pairs differ, including two changes in the disconnected-device set. At 31.25 μs, holding the 8 ms timer for $K_q = 3.0$ leads to unit 1 action at 0.73784375 s; resetting it avoids all actions. Holding the 12 ms timer for $K_q = 3.5$ leads to unit 1 and unit 2 actions at

0.73528125 and 0.736375 s, whereas resetting avoids both. These examples use closed-loop source voltage disturbances rather than prescribed artificial measurement pulses.

Table 12. Refined effects of interruption time and timer reset semantics.

Case and Condition	Action Outcome	Deficit Integral (p.u. s)
Feedback, instantaneous withdrawal	Unit 1 AC	0.296836
Feedback, 0.5 ms withdrawal	Unit 1 AC	0.296649
Feedback, 1 ms withdrawal	Unit 1 AC	0.296466
Feedback, 3 ms withdrawal	Units 1 and 2 AC	0.529921
Two dips, $K_q = 3.0$, 8 ms AC delay, reset	No disconnection	0.083401
Same two dips, timer hold	Unit 1 AC	0.212250
Two dips, $K_q = 3.5$, 12 ms AC delay, reset	No disconnection	0.091688
Same two dips, timer hold	Units 1 and 2 AC	0.340589

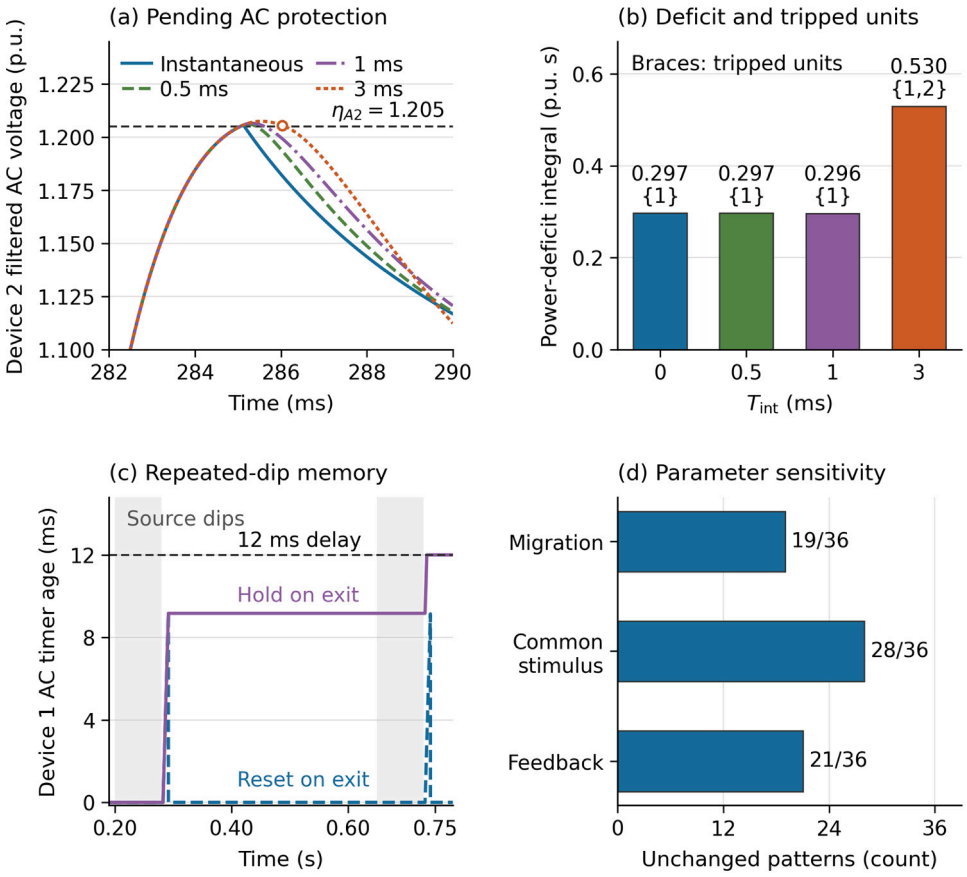


Figure 8. Model assumption sensitivity: (**a**) unit 2 AC protection measurement for different current withdrawal time constants; (**b**) resulting power deficit integrals; (**c**) protection memory under repeated source voltage dips; and (**d**) first cause vector retention under the specified parameter variations.

6.9. Dependence on the Synchronization Model, Control Floor, and Interruption Time

Table 13 repeats the counts of Table 4 for the model variations defined in Section 5.2, with each evaluated at all 1944 points and all eight setting combinations at 62.5 µs. Three observations are common to every variation. No single-setting comparison increases the disconnected unit count, no comparison removes a peer's disconnection, and no point exhibits positive propagation, in which unit 1's original AC action would be necessary for a peer to disconnect. Comparisons that create a new peer action, AC-to-DC changes in the modified unit, suppression points, and nonadditive points occur in every variation.

Within the retained model, the existence of these mechanisms is therefore not a property of the first-order phase model, of the floor value, or of instantaneous withdrawal. The decomposition given in Section 6.1 for the absence of count increases also holds in every variation: outcomes are identical whenever the modified unit was not disconnected by its AC function, no earlier action changes, every disconnection under instantaneous withdrawal lowers the voltages of the surviving units, and no comparison adds more than one peer action, which occurs only when the modified unit remains connected.

The point-level outcomes are model-dependent. With the proportional–integral PLL at a damping ratio of 1.0, 1414 of the 15,552 device sets differ from those of the first-order model; with a damping ratio of 0.707, 2706 differ; and with twice the natural frequency, 7273 differ because the faster loop produces a larger post-clearing overvoltage, as Figure 9a shows for the feedback point. At that point, the two slower PLL settings leave all three units connected, whereas the fastest setting disconnects all three through their AC functions. Of the 269 suppression points of the first-order model, 149, 110, and 104 persist under the three PLL settings and 99, 199, and 553 new ones appear; of the 10 migration points, one, two, and none persist, while eight, 14, and 11 new ones appear. The synchronization model also decides whether the near-boundary cases of Section 6.8 cross the hard limit. The largest AC peak over the grid rises from 1.49999 p.u. with the first-order model to 1.5109, 1.5205, and 1.5210 p.u., and unit 3 reaches its 1.50 p.u. AC hard limit in 256, 712, and 1200 runs at $K_q \geq 3.60$. The 4.3×10^{-6} p.u. margin reported in Section 6.8 is thus confirmed to be no margin at all against a change in the synchronization loop.

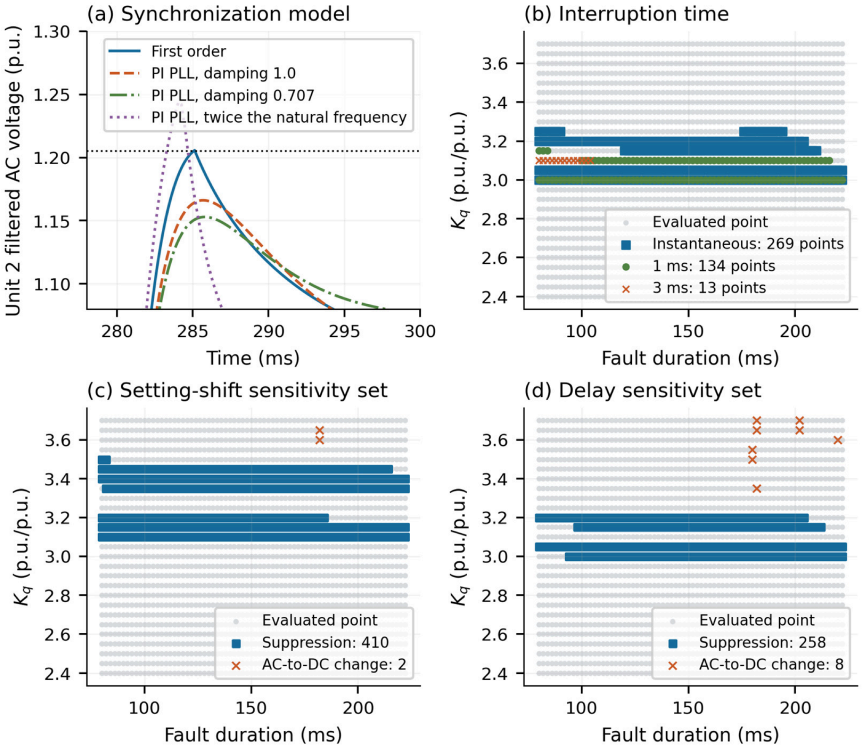


Figure 9. Dependence of the mechanisms on model assumptions and on pre-specified settings: (**a**) unit 2 AC protection measurement at the feedback point for the first-order phase model and the three proportional–integral PLL settings, with the 1.205 p.u. threshold dotted; (**b**) suppression points of the full grid under instantaneous withdrawal and under the assumed first-order interruption law with 1 ms and 3 ms time constants; (**c**) suppression and AC-to-DC migration points of the setting-shift sensitivity set; and (**d**) the same for the delay sensitivity set. Gray dots are evaluated points without the effect.

Table 13. Full-grid outcome counts under the model variations and the two pre-specified sensitivity sets, all at 62.5 µs with 1944 parameter points and eight setting combinations. The first row is the submitted model (first-order phase model, floor 0.05 p.u., and instantaneous withdrawal) and reproduces Table 4. Columns: parameter points with at least one disconnection under the original settings and under all settings changed; points with AC-to-DC migration between these two settings; points at which unit 1's original AC action suppresses a peer's disconnection; among the 23,328 single-setting comparisons, those that create a new peer action, those that replace the modified unit's AC action by a DC action, and those that increase the disconnected unit count; points at which the unit counts are nonadditive; and trajectories of 15,552 that reach a declared hard limit.

Variation	Action Points, Original	Action Points, All Changed	Migration Points	Suppression Points	New Peer Action	AC-to-DC Change	Count Increase	Nonadditive Points	Hard Limit Runs
Submitted model	1224	261	10	269	830	40	0	326	0
PI PLL, $k_p = 65$, damping 1.0	1143	262	9	248	798	36	0	295	256
PI PLL, $k_p = 65$, damping 0.707	1329	349	16	309	1022	64	0	383	712
PI PLL, $k_p = 130$, damping 1.0	1922	454	11	657	2156	44	0	758	1200
Control floor 0.02 p.u.	1224	261	10	269	830	40	0	326	0
Control floor 0.20 p.u.	1224	261	10	269	830	40	0	326	0
Control floor 0.60 p.u.	1224	261	10	269	830	40	0	326	0
Interruption time 1 ms	1224	261	10	134	372	40	0	176	0
Interruption time 3 ms	1224	261	9	13	100	36	0	50	0
Sensitivity set: shifted settings and operating point	1152	90	2	410	1132	8	0	421	0
Sensitivity set: 2 ms AC and 5 ms DC delays	1208	231	8	258	722	32	0	287	8

The control voltage floor changes no action set. Over the grid, the control measurement never falls below 0.419 p.u., so floors of 0.02 and 0.20 p.u. reproduce every trajectory of the submitted model exactly. A floor of 0.60 p.u. binds at 568 points with $K_q \leq 2.75$ and changes their trajectories by at most 0.060 p.u. in peak terminal voltage and 0.0011 p.u. s in deficit integral, but it changes no device set, first cause, or action time: at these gains, the reactive current reference is below its limit, the floor reduces the support slightly, and no threshold is reached, whereas at $K_q \geq 3.0$, the reference saturates at I_{max} before the floor can act. The counts of Table 4 are therefore independent of the floor within the evaluated range.

Under the first-order interruption law of Equation (37), finite interruption time separates the two mechanisms. The AC-to-DC migration points, 10 with instantaneous withdrawal, remain 10 with a 1 ms interruption and nine with 3 ms, and the 40 modified unit AC-to-DC comparisons remain 40 and 36. The suppression points fall from 269 to 134 and 13, and the comparisons with a new peer action from 830 to 372 and 100. Figure 9b shows that only 72 of the original 269 suppression points persist at 1 ms and none at 3 ms; the 13 points found at 3 ms are new ones at $K_q = 3.10$ and short faults. Relative to instantaneous withdrawal, 556 and 904 device sets differ, almost always because an additional unit disconnects: 358 and 613 runs become severe and only 10 and 22 cease to be. Within the averaged model, the loss has the cause identified in Section 6.8 for the single feedback case: the assumed residual current, decaying with the time constant T_{int}, keeps the peer's measured voltage above the threshold long enough for a timer with less than about 1 ms remaining to complete, so the relief that instantaneous withdrawal provides disappears. This explanation and the counts of 269, 134, and 13 points are diagnostic observations of the averaged model under the assumed interruption law; they have not been verified against a circuit-level representation of converter blocking, in which the decay of the current is set by the filter and DC-link circuit, the freewheeling diodes, and the switching sequence, and a different decay could change the counts in either direction. The suppressive-feedback count of Section 6.1 is therefore specific to the assumed withdrawal law, whereas channel migration, the absence of count increases, and nonadditivity are not within the model.

6.10. Pre-Specified Sensitivity Sets

The last two rows of Table 13 report the two pre-specified sensitivity sets. In the setting-shift set, the original settings produce a disconnection at 1152 points and the changed settings at 90; AC-to-DC migration occurs at two points, suppression at 410, and a new peer action in 1132 comparisons, with eight modified unit AC-to-DC changes, 421 nonadditive points, no count increase, and no hard limit contact. In the delay set, with 2 ms AC and 5 ms DC delays, migration occurs at eight points, suppression at 258, and a new peer action in 722 comparisons, with 32 AC-to-DC changes, 287 nonadditive points, no count increase, and one point at which unit 3 reaches the AC hard limit in all eight combinations. Figure 9c,d locates these points. Both sets were evaluated once, without adjustment of their rule-based parameters.

Within the retained model, every mechanism of Sections 6.1–6.6 is therefore also present under settings and operating points that were not used to select the mechanism cases, including the 2 ms delay, for which the exploratory 4 ms scan had found no migration. Their frequencies differ: the shifted settings and the shallower, less phase-shifted disturbance make migration rare and suppression common, while the longer delays reduce every count except that of suppression. The representative points of Sections 6.2 and 6.3 do not transfer: at the 200 ms, $K_q = 3.70$ point, changing only unit 2's threshold leaves it connected in both sets, and at the 80 ms, $K_q = 3.00$ point, changing unit 1's threshold no longer disconnects unit 2. A mechanism case identified in one setting therefore remains a case for that setting; the sensitivity sets show that the mechanisms persist within the retained model under these

pre-specified changes, but not that individual points transfer, and, because they belong to the same benchmark and were chosen by the authors, they do not constitute independent out-of-sample validation.

7. Discussion

The numerical study supports a protection state interpretation of correlated disconnection. This section separates the implications that follow from the calculated mechanisms from the additional evidence needed for engineering protection decisions. The central distinction is among avoiding a particular channel, retaining a particular device, and satisfying equipment limits after the action; none of these outcomes should be substituted for either of the others.

7.1. Implications for Disturbance Assessment

The complete intervention comparisons show why a single disconnected unit count is insufficient. A setting change can keep the modified unit connected while shifting the disconnection to another unit. Channel competition can preserve the same terminal device set while changing the first cause. Deficit integrals can increase even when counts do not. A useful study record therefore includes the device identities, initiating functions, times, and post-action energy states together with aggregate consequences.

Protection timing is also part of the electrical response. Faster local action can reduce the stimulus seen by other units, so a zero-delay approximation can underestimate multiple disconnections. Conversely, resetting a surviving timer at another unit's action erases already accumulated exposure. The conditional filter bounds explain both completion despite a low instantaneous voltage and reset following sufficient network relief. When the input information is too broad, unresolved outcomes appropriately preserve the need for further trajectory calculation.

The post-blocking energy result supplies a complementary constraint. The source exit time constant is meaningful only together with the capacitor energy and source power at blocking. A fixed source response number cannot be classified as adequate independently of those states. Where residual port current persists, the associated AC energy transfer must be included. This connects protection assessment to the physical interruption process without assuming that one averaged interruption law represents every converter topology.

7.2. Classification of the Findings

Table 14 separates the findings by the evidence that supports them. A finding is classed as invariant within the retained model when it holds for every model variation and pre-specified sensitivity set of Sections 6.9 and 6.10, preferably with a structural explanation, such as that given in Section 6.1. This class describes the retained equations and the evaluated grids and does not imply physical robustness, which only EMT, hardware, or field evidence can establish. This class is established as model-dependent when its value, or its presence at a given point, changes under those variations; moreover, it is established as requiring EMT or hardware validation when the present model cannot represent the physics that decides it.

Table 14. Classification of the findings by the evidence that supports them.

Finding	Class	Evidence
No bounded local AC setting change increases the disconnected unit count, and none removes a peer's disconnection	Invariant within the retained model	Zero of 23,328 comparisons in every variation and sensitivity set (Table 13); structural explanation in Section 6.1
A local AC setting change can shift the disconnection to a peer or replace an AC action by a DC action	Invariant within the retained model	100–2156 new-peer and 8–64 AC-to-DC comparisons in every variation and set
Effects of separate local changes do not add	Invariant within the retained model	50–758 nonadditive points in every variation and set; accounting identity of Equation (36)
Pending AC timers complete under sub-threshold terminal voltage because of measurement lag and retained age	Invariant within the retained model	24 of 64 completions; Equation (19); definite time relay logic
Sign and size of the instantaneous voltage change at a disconnection	Exact within the algebraic network	Equation (14); residual 1.6×10^{-16} p.u.
Residual energy boundary and delayed DC violation after blocking	Exact within the source model; value depends on the blocking state	Equations (23)–(25); 99.267 ms for the examined state
Suppressive network feedback at a given point, and its count of 269 points	Model-dependent	Diagnostic observation of the averaged model: 134 and 13 points at 1 and 3 ms interruption under the assumed law; 248–657 under the PI PLL; no original point persists at 3 ms
Point-level device sets, first causes, and the representative cases	Model-dependent	9–47% of device sets change with the synchronization model; representative points do not transfer to the sensitivity sets
Severe outcome counts of the protection model comparison	Threshold- and resolution-dependent	Table 9; 34 severe labels change between 250 and 62.5 µs
Hard limit non-exceedance of the near-boundary band	Not robust	4.3×10^{-6} p.u. margin; 256–1200 AC hard contacts under the PI PLL
Effect of negative sequence quantities, switching ripple, and the actual interruption circuit on the channel competition	Requires EMT or hardware validation	Not represented; the finite interruption law is a sensitivity assumption
Transfer to plant-specific settings, measuring windows, and field conditions	Requires EMT or hardware validation	No manufacturer, field-recording, or detailed EMT data in this study

7.3. Contribution and Applicability

The assessment combines known network and first-order dynamic identities with a complete conditional setting comparison. Its contribution is a model-specific diagnostic framework: the joint, trajectory-consistent treatment of protection state memory, competing causes, network feedback, and residual energy constraints in one reproducible evaluation, together with the quantification of how often each mechanism changes the outcome on a common test case. The comparison with the fixed-topology relay evaluation in Section 6.7 shows what that conventional evaluation omits on the same benchmark; it is a logical necessity check within the same equations and does not show that the full model is physically

closer to reality. A comparison with a detailed EMT assessment of the same case, which could provide such evidence, has not been made and is identified below as the next validation step. The finite differences provide a transparent measure of nonadditive local setting effects; the conditional inequalities give interpretable reasons for individual pending-timer outcomes. Neither construction is presented as a new universal stability theorem.

For an engineering study, the same calculation requires actual measurement filters, timer reset semantics, limits, source controls, and interruption behavior. A time-ordered list of recorded disconnections can suggest comparisons, but does not supply those states. Diagnostic setting changes must also remain separate from field recommendations: a threshold acceptable in the retained model might violate detection, selectivity, ride-through, or equipment requirements omitted from it. The present results identify information that such a decision needs rather than selecting deployment settings.

7.4. Limitations and Further Validation

The system has three aggregated grid-following converters and a balanced positive sequence algebraic network. It omits negative sequence regulation, detailed synchronization controllers, PWM, filter inductance and capacitor transients, diode conduction, semiconductor limits, breaker behavior, plant-level controls, synchronous machine dynamics, and multi-terminal DC interactions. The finite interruption time variation exposes one dependence on these omissions but does not validate a particular interruption circuit. There are no manufacturer, field-recording, controller-hardware, or detailed EMT results in this study.

The finite setting set and deterministic parameter grid provide neither complete continuous-domain reachability nor a robust guarantee under unknown firmware or measurement error. Representative cases were selected to explain mechanisms after initial parameter exploration; the two sensitivity sets of Section 6.10 were specified by rule before evaluation, but they remain finite grids of the same benchmark, chosen by the authors, and are not independent out-of-sample validation. Some model outcomes and classification counts change with integration step. Conditional forward envelopes depend on valid slope and fixed-topology assumptions, and the slope bound of Equation (21) must be rederived for a second-order synchronization loop; retrospective envelopes use future trajectory information. Their agreement with numerical solutions does not establish validated numerics for every continuous trajectory.

Which conclusions are expected to remain valid when detailed synchronization, inner current-loop, negative sequence, and switching dynamics are included can be stated from their derivation. The separation of the three checks, the sign relation of the network jump, and the completion of a timer under sub-threshold terminal voltage follow from the algebraic positive sequence network and from definite time relay logic acting on a lagging measurement; they are expected to persist whenever the relay acts on a filtered positive sequence magnitude, although the size of the lag depends on the actual measuring window. The absence of count increases rests on the three structural features identified in Section 6.1, namely the monotone response of a definite time element to its pick-up value, the voltage relief given by every disconnection, and the one-for-one substitution of the modified unit by at most one peer; it is expected to persist only where these features hold. The grid-level counts, the identity of the affected unit at a given point, and the direction of the feedback at a given point depend on the closed-loop voltage trajectory after clearing and are therefore model-dependent; Section 6.9 measures how far they move when the synchronization loop or the interruption law changes, and the inner current loop enters through T_I, whose variation is part of Table 11. Negative sequence components and switching ripple enter the measured quantities themselves and can advance or delay both channels; their effect on

the competition cannot be inferred from the present model and requires EMT or hardware testing. Table 14 records this classification finding by finding.

Further engineering validation should substitute independently specified converter and relay implementations, preserve the DC power balance during physical blocking, and test asymmetrical and repeated faults with measured control parameters. A held-out set of operating points, disturbance locations, and settings that are not chosen by the authors is needed before using the method for plant-specific judgments. Detailed EMT and controller or relay testing should compare both the continuous waveforms and the action state sequence. Failure to reproduce a cause or timer reset is material even when the total disconnected capacity is similar.

8. Conclusions

This paper asked which converters of a group sharing a weak common bus disconnect after a fault, through which protective function, and how the first disconnection changes the actions of the others. The answers to these questions, within the constructed benchmark, are found within a protection state interpretation of correlated disconnection. The post-fault overvoltage produced by reactive current support starts the AC overvoltage timers of all units, while the energy accumulated during the fault drives their DC overvoltage functions. The first disconnection removes a current from the common bus and lowers the terminal voltages of the others at once, but their relay measurements lag that change and their timers retain the exceedance already accumulated. Whether a peer then disconnects is decided by the race between its remaining timer duration and the measurement lag, and whether the modified unit stays connected is decided by its competing DC channel. A hybrid state carrying continuous converter states, filtered measurements, timer ages, connection states, and first-cause latches is the information from which these outcomes can be reproduced.

The findings hold under the stated assumptions: a balanced positive sequence network, aggregated current-controlled converters, definite time protective functions acting on first-order filtered magnitudes, converter blocking with latched disconnection, and the evaluated parameter grid. Within them, three findings are invariant under the synchronization model, the control voltage floor, the current interruption time, and two pre-specified sensitivity sets of the same benchmark; this invariance concerns the retained model and is not evidence of physical robustness: no bounded local AC setting change increases the disconnected unit count, which is a consequence of the monotone response of a definite time element to its pick-up value, of the voltage relief given by every disconnection, and of the one-for-one substitution of the modified unit by at most one peer, yet such changes shift the disconnection to a peer in hundreds of comparisons and replace an AC action by a DC action in tens; the effects of separate local changes do not add; and pending AC timers complete under sub-threshold terminal voltage because of measurement lag and retained age. The residual energy relation adds that a blocked unit can violate its DC limit long after disconnection, with a critical source exit time constant of 99.267 ms for the examined blocking state. The fixed-topology relay evaluation of conventional multi-outage studies reproduces whether any unit disconnects but gives a different device set in 613 of 5832 runs and cannot represent suppressive feedback; because it uses the same equations, this comparison is a logical necessity check of what omitting the feedback implies, not independent evidence that the full model is physically closer to reality.

Other findings are model-dependent and are reported as such. Under the first-order interruption law assumed in the averaged model, the suppressive network feedback found at 269 points under instantaneous current withdrawal persists at 134 points for a 1 ms and at 13 points for a 3 ms interruption; within that model, the decaying residual current keeps the peer's measurement above the threshold long enough for its timer to complete.

These counts and this explanation are diagnostic observations conditioned on the assumed interruption law and have not been verified with a circuit-level representation of the interruption. A proportional–integral synchronization loop changes 9–47% of the device sets, moves individual mechanism cases to other points, and carries the near-boundary cases over the 1.50 p.u. AC hard limit, so the nominal non-exceedance of the submitted model is not a safety margin. Severe outcome counts depend on the chosen threshold and on the integration step.

The assessment is a model-specific diagnostic framework. It identifies the states and model information that a plant-specific protection judgment requires and the comparisons that reveal when a setting change merely moves a disconnection, but it does not provide protection settings, outage probabilities, or a replacement for detailed converter, relay, and field validation. The effects of negative sequence quantities, switching ripple, and the actual interruption circuit on the channel competition and on the suppressive feedback remain to be established with EMT or hardware tests.

Author Contributions: Conceptualization, F.L. and J.Q.; methodology, F.L.; software, F.L. and H.L.; validation, F.L. and H.L.; formal analysis, J.Q.; investigation, J.M. and R.S.; resources, J.M. and G.G.; writing—original draft preparation, F.L. and J.Q.; writing—review and editing, H.L. and J.M.; visualization, R.S. and G.G. All authors have read and agreed to the published version of the manuscript.

Funding: This research was funded by the Technology Service Project of the State Grid Corporation of China (Research on Power Grid Development Planning for the 15th Five-Year Plan Period—Research on Planning Schemes), grant number B3440825G027. The funders had no role in the design of the study; in the collection, analyses, or interpretation of data; in the writing of the manuscript; or in the decision to publish the results.

Data Availability Statement: The original contributions presented in this study are included in the article. Further inquiries can be directed to the corresponding author.

Conflicts of Interest: Authors Fan Li, Jishuo Qin, Hanqing Liang, Jian Meng, and Guodong Guo were employed by the State Grid Economic and Technology Research Institute Co., Ltd. Author Rui Shi was employed by the State Grid Corporation of China. The remaining authors declare that the research was conducted in the absence of any commercial or financial relationships that could be construed as potential conflicts of interest. The authors declare that this study received funding from the State Grid Corporation of China. The funder was not involved in the study design, collection, analysis, interpretation of data, the writing of this article, or the decision to submit it for publication.

References

1. Blaabjerg, F.; Teodorescu, R.; Liserre, M.; Timbus, A.V. Overview of Control and Grid Synchronization for Distributed Power Generation Systems. *IEEE Trans. Ind. Electron.* **2006**, *53*, 1398–1409. [CrossRef]
2. Wang, X.; Taul, M.G.; Wu, H.; Liao, Y.; Blaabjerg, F.; Harnefors, L. Grid-Synchronization Stability of Converter-Based Resources—An Overview. *IEEE Open J. Ind. Appl.* **2020**, *1*, 115–134. [CrossRef]
3. Zha, X.; Huang, M.; Liu, Y.; Tian, Z. An overview on safe operation of grid-connected converters from resilience perspective: Analysis and design. *Int. J. Electr. Power Energy Syst.* **2022**, *143*, 108511. [CrossRef]
4. Mirhosseini, M.; Pou, J.; Agelidis, V.G. Single- and Two-Stage Inverter-Based Grid-Connected Photovoltaic Power Plants with Ride-Through Capability Under Grid Faults. *IEEE Trans. Sustain. Energy* **2015**, *6*, 1150–1159. [CrossRef]
5. Ding, G.; Gao, F.; Tian, H.; Ma, C.; Chen, M.; He, G.; Liu, Y. Adaptive DC-Link Voltage Control of Two-Stage Photovoltaic Inverter During Low Voltage Ride-Through Operation. *IEEE Trans. Power Electron.* **2016**, *31*, 4182–4194. [CrossRef]
6. Wang, Y.; Ren, B. Fault Ride-Through Enhancement for Grid-Tied PV Systems with Robust Control. *IEEE Trans. Ind. Electron.* **2018**, *65*, 2302–2312. [CrossRef]
7. Taul, M.G.; Wang, X.; Davari, P.; Blaabjerg, F. An Overview of Assessment Methods for Synchronization Stability of Grid-Connected Converters Under Severe Symmetrical Grid Faults. *IEEE Trans. Power Electron.* **2019**, *34*, 9655–9670. [CrossRef]
8. Wu, H.; Wang, X. Design-Oriented Transient Stability Analysis of PLL-Synchronized Voltage-Source Converters. *IEEE Trans. Power Electron.* **2020**, *35*, 3573–3589. [CrossRef]

9. Zhao, J.; Huang, M.; Yan, H.; Tse, C.K.; Zha, X. Nonlinear and Transient Stability Analysis of Phase-Locked Loops in Grid-Connected Converters. *IEEE Trans. Power Electron.* **2021**, *36*, 1018–1029. [CrossRef]
10. He, X.; Geng, H.; Li, R.; Pal, B.C. Transient Stability Analysis and Enhancement of Renewable Energy Conversion System During LVRT. *IEEE Trans. Sustain. Energy* **2020**, *11*, 1612–1623. [CrossRef]
11. Hu, Q.; Fu, L.; Ma, F.; Ji, F.; Zhang, Y. Analogized Synchronous-Generator Model of PLL-Based VSC and Transient Synchronizing Stability of Converter Dominated Power System. *IEEE Trans. Sustain. Energy* **2021**, *12*, 1174–1185. [CrossRef]
12. He, X.; He, C.; Pan, S.; Geng, H.; Liu, F. Synchronization Instability of Inverter-Based Generation During Asymmetrical Grid Faults. *IEEE Trans. Power Syst.* **2022**, *37*, 1018–1031. [CrossRef]
13. Liu, Y.; Zhu, L.; Xu, X.; Li, D.; Liang, Z.; Ye, N. Transient Synchronization Stability in Grid-Following Converters: Mechanistic Insights and Technological Prospects—A Review. *Energies* **2025**, *18*, 1975. [CrossRef]
14. Banaiemoqadam, A.; Hooshyar, A.; Azzouz, M.A. A Comprehensive Dual Current Control Scheme for Inverter-Based Resources to Enable Correct Operation of Protective Relays. *IEEE Trans. Power Deliv.* **2021**, *36*, 2715–2729. [CrossRef]
15. Fan, B.; Liu, T.; Zhao, F.; Wu, H.; Wang, X. A Review of Current-Limiting Control of Grid-Forming Inverters Under Symmetrical Disturbances. *IEEE Open J. Power Electron.* **2022**, *3*, 955–969. [CrossRef]
16. Zhang, H.; Ma, J.; Li, X. Dynamic Current-Limitation Strategy of Grid-Forming Inverters Based on SR Latches. *Electronics* **2024**, *13*, 3432. [CrossRef]
17. Bottrell, N.; Green, T.C. Comparison of Current-Limiting Strategies During Fault Ride-Through of Inverters to Prevent Latch-Up and Wind-Up. *IEEE Trans. Power Electron.* **2014**, *29*, 3786–3797. [CrossRef]
18. Ordono, A.; Sanchez-Ruiz, A.; Zubiaga, M.; Asensio, F.J.; Cortajarena, J.A. Current limiting strategies for grid forming inverters under low voltage ride through. *Renew. Sustain. Energy Rev.* **2024**, *202*, 114657. [CrossRef]
19. Gwon, D.; Choi, Y. Reactive Power Based Fault Ride Through Control of IBR-Dominated Distribution Networks Under Low WSCR. *Electronics* **2026**, *15*, 521. [CrossRef]
20. Phadke, A.G. Hidden failures in electric power systems. *Int. J. Crit. Infrastruct.* **2004**, *1*, 64–75. [CrossRef]
21. Chen, J.; Thorp, J.S.; Dobson, I. Cascading dynamics and mitigation assessment in power system disturbances via a hidden failure model. *Int. J. Electr. Power Energy Syst.* **2005**, *27*, 318–326. [CrossRef]
22. Song, J.; Cotilla-Sanchez, E.; Ghanavati, G.; Hines, P.D.H. Dynamic Modeling of Cascading Failure in Power Systems. *IEEE Trans. Power Syst.* **2016**, *31*, 2085–2095. [CrossRef]
23. Hines, P.D.H.; Dobson, I.; Rezaei, P. Cascading Power Outages Propagate Locally in an Influence Graph that is not the Actual Grid Topology. *IEEE Trans. Power Syst.* **2017**, *32*, 958–967. [CrossRef]
24. Dobson, I.; Carreras, B.A.; Lynch, V.E.; Newman, D.E. Complex systems analysis of series of blackouts: Cascading failure, critical points, and self-organization. *Chaos* **2007**, *17*, 026103. [CrossRef] [PubMed]
25. Nakarmi, U.; Rahnamay Naeini, M.; Hossain, M.J.; Hasnat, M.A. Interaction Graphs for Cascading Failure Analysis in Power Grids: A Survey. *Energies* **2020**, *13*, 2219. [CrossRef]
26. Li, H.; Yu, H.; Liu, Z.; Li, F.; Wu, X.; Cao, B.; Zhang, C.; Liu, D. Long-term scenario generation of renewable energy generation using attention-based conditional generative adversarial networks. *Energy Convers. Econ.* **2024**, *5*, 15–27. [CrossRef]
27. Hiskens, I.A.; Pai, M.A. Trajectory sensitivity analysis of hybrid systems. *IEEE Trans. Circuits Syst. I Fundam. Theory Appl.* **2000**, *47*, 204–220. [CrossRef]
28. Golestan, S.; Guerrero, J.M.; Vasquez, J.C. Three-Phase PLLs: A Review of Recent Advances. *IEEE Trans. Power Electron.* **2017**, *32*, 1894–1907. [CrossRef]
29. Phadke, A.G.; Thorp, J.S. *Computer Relaying for Power Systems*, 2nd ed.; Wiley: Chichester, UK, 2009.
30. *IEC 60255-127:2010*; Measuring Relays and Protection Equipment—Part 127: Functional Requirements for Over/Under Voltage Protection. International Electrotechnical Commission: Geneva, Switzerland, 2010.
31. *IEEE Std 1547-2018*; IEEE Standard for Interconnection and Interoperability of Distributed Energy Resources with Associated Electric Power Systems Interfaces. IEEE: Piscataway, NJ, USA, 2018.

Disclaimer/Publisher's Note: The statements, opinions and data contained in all publications are solely those of the individual author(s) and contributor(s) and not of MDPI and/or the editor(s). MDPI and/or the editor(s) disclaim responsibility for any injury to people or property resulting from any ideas, methods, instructions or products referred to in the content.